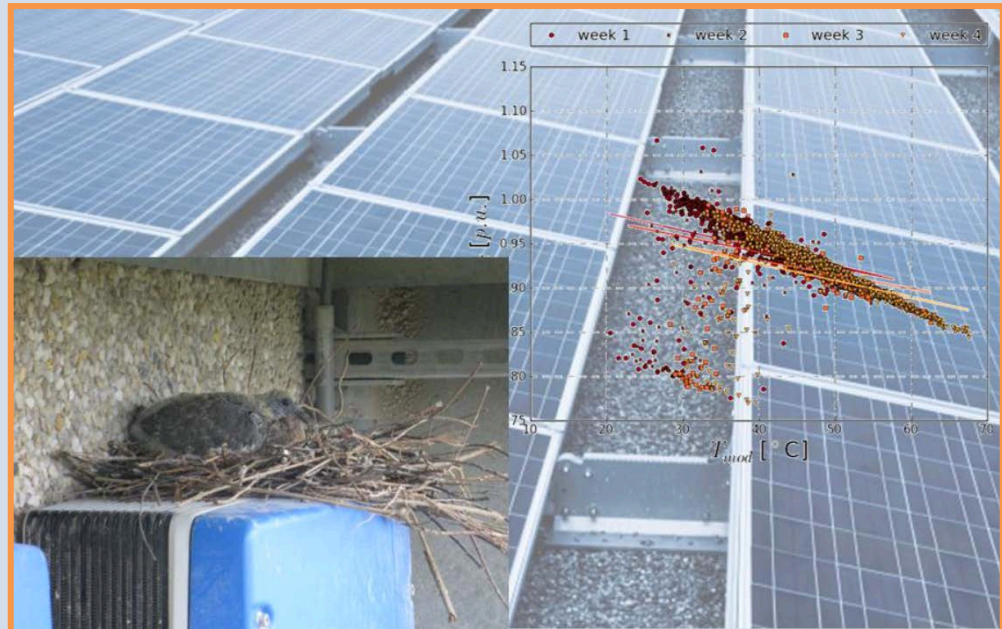IEA-PVPS

Analytical Monitoring of Grid-connected Photovoltaic Systems

Good Practices for Monitoring and Performance Analysis

PVPS

PHOTOVOLTAIC POWER SYSTEMS PROGRAMME

Report IEA-PVPS T13-03:2014

INTERNATIONAL ENERGY AGENCY
PHOTOVOLTAIC POWER SYSTEMS PROGRAMME

Analytical Monitoring of Grid-connected Photovoltaic Systems

Good Practices for Monitoring and Performance Analysis

Authors:

Achim Woyte & Mauricio Richter, 3E, Belgium, achim.woyte@3e.eu
David Moser, EURAC research, Italy, david.moser@eurac.edu
Nils Reich, Fraunhofer ISE, Germany, nils.reich@ise.fraunhofer.de
Mike Green, M.G.Lightning Electrical Engineering, Israel, mike@lightning.co.il
Stefan Mau, GL Garrad Hassan, Spain, stefan.mau@gl-garradhassan.com
Hans Georg Beyer, University of Agder, Norway, hans-georg.beyer@uia.no

Acknowledgements

Foreword

The International Energy Agency (IEA), founded in November 1974, is an autonomous body within the framework of the Organization for Economic Co-operation and Development (OECD) which carries out a comprehensive programme of energy co-operation among its member countries. The European Union also participates in the work of the IEA. Collaboration in research, development and demonstration of new technologies has been an important part of the Agency's Programme.

The IEA Photovoltaic Power Systems Programme (PVPS) is one of the collaborative R&D Agreements established within the IEA. Since 1993, the PVPS participants have been conducting a variety of joint projects in the application of photovoltaic conversion of solar energy into electricity.

The mission of the IEA PVPS programme is: To enhance the international collaborative efforts which facilitate the role of photovoltaic solar energy as a cornerstone in the transition to sustainable energy systems.

The underlying assumption is that the market for PV systems is rapidly expanding to significant penetrations in grid-connected markets in an increasing number of countries, connected to both the distribution network and the central transmission network.

This strong market expansion requires the availability of and access to reliable information on the performance and sustainability of PV systems, technical and design guidelines, planning methods, financing, etc., to be shared with the various actors. In particular, the high penetration of PV into main grids requires the development of new grid and PV inverter management strategies, greater focus on solar forecasting and storage, as well as investigations of the economic and technological impact on the whole energy system. New PV business models need to be developed, as the decentralized character of photovoltaics shifts the responsibility for energy generation more into the hands of private owners, municipalities, cities and regions.

The overall programme is headed by an Executive Committee composed of representatives from each participating country and organization, while the management of individual research projects (Tasks) is the responsibility of Operating Agents. By late 2013, fourteen Tasks were established within the PVPS programme, of which six are currently operational.

The overall objective of Task 13 is to improve the reliability of photovoltaic systems and subsystems by collecting, analysing and disseminating information on their technical performance and failures, providing a basis for their assessment, and developing practical recommendations for sizing purposes.

The current members of the IEA PVPS Task 13 include:

Australia, Austria, Belgium, China, EPIA, France, Germany, Israel, Italy, Japan, Malaysia, Netherlands, Norway, Spain, Sweden, Switzerland, Turkey and the United States of America.

This report focusses on analytical PV monitoring, including current best practices of both the technical setup of PV monitoring installations and subsequent analysis procedures. Due to the wealth of measured data from operational PV systems available for this report it also aims to further develop documented best practices, entailing design and component selection aspects of PV monitoring system, the determination of physical relationships of parameters influencing PV performance, and finally the use of computer simulation approaches to calculate parameters of PV system losses that cannot be directly measured. Both the impact of system design decisions on PV performance and best practices of PV monitoring include particularities of special technologies.

Systematically applied, the set of practical guidelines, methods and models presented in this report will help to understand PV performance issues and assure or even increase the performance of PV power plants in the future.

The editors of the document are Achim Woyte, 3E, Brussels, Belgium, and Nils H. Reich, Fraunhofer ISE, Freiburg, Germany.

The report expresses, as closely as possible, the international consensus of opinion of the Task 13 experts on the subject dealt with. Further information on the activities and results of the Task can be found at: http://www.iea-pvps.org.

Executive Summary

This report focuses on the analytical assessment of photovoltaic (PV) plant performance on the overall PV system level. In particular, this report provides detailed guidelines and comprehensive descriptions of methods and models used when analyzing grid-connected PV system performance.

The main objectives of this report are:
- to propose good practices for PV system monitoring today,
- to determine and understand PV system losses that cannot be assessed by direct measurements in commercial PV systems,
- to determine and understand the behavior of new PV technologies in long-term system operation,
- to learn from previous bad experiences and draw out lessons for new installations in the IEA PVPS member countries.

In the starting section, "Photovoltaic System Monitoring", best practices in PV monitoring are documented. In addition to describing general monitoring approaches and listing common reference documents, the section outlines peculiarities of different measurement equipment and highlights best practices for hardware configuration and installation. An overview of various interesting measurement quantities and related failure patterns is also provided.

In the second section, "Understanding Photovoltaic System Operation through Monitoring", comprehensive guidelines on how to analyze performance data are given, based on concrete examples using periodic linear regression. The section highlights the versatility of this linear-regression-based approach for PV performance analysis. The approach can, for example, be used to assess the influence of module temperature on array and system performance, the influence of wind speed, DC voltage deviations and their relation to module temperature, as well as the resilience of grid voltage to active power.

The majority of presented methods and tools can be applied irrespective of particular module technologies. However, a number of special effects related to less common module technologies require some consideration, as outlined in a dedicated chapter on "new" technologies. In particular, CIGS and amorphous silicon modules have been analyzed in this study. Based on data from different experimental installations in the field, the specific behavior of the new modules was modeled and compared to classical crystalline silicon PV. The existing models for crystalline silicon require major modifications especially for modules involving amorphous silicon. This is detailed in the third chapter, "Understanding Effects Related to Special Technologies".

Finally, measures that can help improve the performance of PV systems are described in the fourth chapter, "PV System Performance Improvement". This section outlines recommendations for improvement, based on lessons learned from PV system design over the past decade. To this end, a brief introduction to traditional performance indicators is given, along with an overview of the trends in PV system performance over the years. Key system design decisions, such as

mounting angle and row distance, inverter to module power ratio, and cabling optimizations, are also addressed. Several examples on both shading losses and inverter to module power ratio are highlighted, providing deeper insight into the pitfalls and merits of various system design options. Finally, the basic approach of real-time data processing is described as a means to optimize system output by increased responsiveness to outages.

The full report delivers a comprehensive set of practical guidelines for analytical PV system monitoring. Applied systematically, these guidelines will contribute to further increasing the performance of PV power plants.

Table of Contents

1 Photovoltaic System Monitoring

1.1 State of the Art

The main purposes of a monitoring system are to measure the energy yield, to assess the PV system performance and to quickly identify design flaws or malfunctions. Many large PV systems use analytical monitoring to prevent economic losses due to operational problems.

As specified by [1] and [2], the requirements for so-called analytical or detailed monitoring include an automatic dedicated data acquisition system with a minimum set of parameters to be monitored. A study of failures for grid-connected residential PV systems of 1-5 kWp installed in Germany in the 1990's [3] found that a statistical failure happened every 4.5 years per plant. Inverters contributed 63%, PV modules 15% and other system components 22% to the total failures. An adequate monitoring system can allow the timely detection of operational problems, thus warranting a higher final energy yield than would be possible without monitoring.

Task 2 of the IEA PVPS has gathered and analyzed monitoring data from several countries world-wide. This work yielded a comparative study of PV system performance in different countries over many years and a number of new approaches and analysis methods for PV system performance measurements [4]. The results presented in [5] have shown that several PV systems installed before 1994 did not generate the expected energy yield. However, due to realistic PV module ratings, better inverter efficiencies and higher system availabilities, a clear tendency towards improved performance was found for new PV installations installed after 1996. A lack of long-term experiences in performance and reliability of PV systems has been identified and linked to a lack of detailed and more reliable monitoring campaigns [5], [6].

Common reference documents for monitoring of PV systems are the standard IEC 61724 [1] and the guidelines of the European Joint Research Centre in Ispra, Italy [2], [7]. As stated by [1] and [2], the requirements for what they call analytical or detailed monitoring include an automatic dedicated data acquisition system with a minimum set of parameters to be monitored.

From the parameters listed in [1], those concerning grid-connected PV systems are summarized below in Table 1 and shown also in Figure 6.

The required accuracies and check procedures for data quality are detailed in [1], [2] and [7]. According to current standards [1], [2], the in-plane irradiance should be measured with a crystalline silicon reference device, which should be calibrated and maintained in accordance with IEC 60904-2 or IEC60904-6. However, more recent studies such as [8] and [9] have shown that the use of silicon reference devices for PV performance evaluation can lead to uncertainties that cannot easily be quantified. Thus the use of a thermopile pyranometer for PV performance evaluation is recommended.

Table 1: Parameters to be measured in real time (adapted from [1])

Parameter	Symbol	Unit
In-plane Irradiance	G_I	W/m^2
Ambient temperature	T_{amb}	°C
Module temperature	T_{mod}	°C
Wind speed	S_w	m/s
PV array output voltage	V_{DC}	V
PV array output current	I_{DC}	A
PV array output power	P_{DC}	kW
Utility grid voltage	V_{AC}	V
Current to utility grid	I_{AC}	A
Power to utility grid	P_{AC}	kW
Durations of system outage	t_{outage}	s

Monitoring guidelines should provide clear instructions on how to conduct and analyze the measurements and how to determine whether the system is performing as expected. As stated by [10] and [11], the current recommendations and guidelines for the measurements and analysis of the performance of PV systems ([1], [2], [7]), were originally developed to establish the main operating characteristics of systems in demonstration projects without providing any guidance for reducing output losses over system lifetime. As part of the European Commission-funded project PERFORMANCE, new PV monitoring guidelines have been developed and presented within a spreadsheet tool [10] and a method based on failure mode analysis was presented [12]. These new monitoring guidelines are meant to "meet the different market needs, including lifetime monitoring and timely detection of faults" [10]. However, up to now these guidelines have not yet been applied widely. Routines for automatic failure detection from monitoring data during operations have been presented, e.g. in [13], [14] and [15].

A Failure Detection Routine (FDR) for comparing the monitored energy yield with the simulated one for a given period was presented in [14] and [15]. The FDR consists basically of three parts: the failure detection system, the failure profiling method and the footprint method. If the monitored energy yield is significantly lower than the simulated energy yield, a failure is identified. The FDR evaluates the pattern of the energy loss by creating a profile of the actual failure and comparing it with predefined profiles of several frequently occurring failures. Depending on the correlation between the actual failure profile and the predefined profiles, the FDR assesses the likelihood of different failures. The footprint method serves for analysis of patterns in dependency of three different domains: normalized monitored power, time (hour of the day), and sun elevation. The footprint method has been developed by analyzing typical system faults using data of well monitored PV plants within the German 1000-roofs program.

The predefined 12 failure patterns and the analyzed aspects in the FDR are summarized in Table 2. The first results of the FDR as stated in [14] show that the methodology is good at finding out which failures are absolutely impossible, but fine tuning is still needed. Field tests [16] have shown that it can take between one day and several months to detect a failure for the PVSAT-2 routine [17] that applies the FDR methodology, depending mainly on weather conditions, size and continuity of the failures.

Table 2: Failure patterns and analyzed aspects of the FDR [14] [15]

Failure	Analyzed aspects for each failure
1. Degradation / module over rating 2. Soiling 3. Module defect 4. String defect 5. Snow cover 6. Hot modules 7. Shading 8. Part load behavior 9. Maximum power point (MPP) tracking 10. Grid outage 11. Defect inverter 12. Defect control devices	• Daily energy loss • Hourly energy loss • Temperature during last 3 days • Spatial dimension (neighboring PV systems) • Changes behavior (e.g. constant energy loss) • Duration • Correlation with sun elevation and irradiance (i.e. footprint method [15])

Another example of automatic failure detection from monitoring data is the Sophisticated Verification Method (SV method) of PV systems [13]. The latest version of this method allows identifying 12 different loss factors based on the fundamental system specifications and data for seven simple measurable quantities [18]. The system losses and basic input data are summarized in Table 3.

Table 3: Measured operational data and system losses identified by the SV method (from [18], nomenclature adapted)

Measured operational quantities	System loss rates
1. PV array output current 2. PV array output voltage 3. Power to utility grid 4. Current to utility grid 5. Utility grid voltage 6. Module temperature 7. Irradiation data from meteo stations	1. Inverter 2. Module temperature 3. Inverter capacity shortage 4. Grid voltage 5. Operating point mismatch 6. Fluctuation 7. Inverter off/stand-by 8. Reflection 9. DC circuit resistance 10. Shading 11. System peak power loss 12. Miscellaneous loss

Based on the extended collection of monitoring data from the IEA PVPS Task 2, the performance of 21 grid-connected PV systems, which have been operational between seven and 23 years, has been compared [4]. The 21 PV systems are located in five different European countries as well as Japan and were selected to understand and improve the understanding of operational PV system behavior. Graphical analysis methods were used to identify energy frequency distributions and the performance ratio (*PR*) was analyzed to detect small shifts of system performance. Through a collection of plots and interpretation guidelines (e.g., plotting final yield versus reference yield, DC voltage versus power, *PR* over time and *PR* versus module temperature), the authors show how different system behavior affects the *PR*. They confirmed that, since values at identical climatic

conditions show little scattering, the *PR* is the most useful quantity for detecting even small variations of system performance.

A similar study [19] presents a collection of plots and interpretation guidelines by using different combinations of scatter plots and time series plots. Values modeled with empirical formulae are compared with measured data and some operational problems are covered, e.g., shading issues and voltage miss-tracking, due to inverter overheating in this case. It has been found that the DC module performance can be characterized by frequent measurements of "performance factor" (DC efficiency measured / efficiency at STC) [20] versus in-plane irradiance, temperature and wind speed. Voltage miss-tracking and shading issues can be identified by plotting the normalized voltage and current against time or in-plane irradiance.

1.2 Instruments and Required Precision

This section deals with the sensors and uncertainties that are required for monitoring utility scale PV plants.

Appropriate monitoring of a PV plant is necessary to manage its operation and performance. In the case of utility scale PV plants this means often a comparison of the current plant performance with an initial energy yield assessment. To analyze the profitability and the energy yield of a utility scale PV plant, the measurement of the generated energy at the revenue meter located at the connection point assigned by the utility would be sufficient. However, without further information it is not possible to conclude whether low production is due to underperformance or a period with less irradiation than expected. For that reason, any monitoring should include both a measurement of the energy generated and the incoming irradiation.

The following is an analysis of the irradiation sensors, together with a review of the energy generation measurements for PV plant performance monitoring.

When selecting irradiation sensor technology, generally only two possibilities exist: thermopile sensors (pyranometer) or solar cell sensors. In solar cells, only crystalline silicon sensors provide the required stability. No long-term stable irradiation sensors exist for CIS, amorphous silicon and CdTe [21]. In case of amorphous silicon (single junction), a silicon based sensor with a filter glass can be used as it has a similar spectral response.

Thermopile sensors (Pyranometers)
Pyranometers are based on a thermocouple device. When heated by the incident irradiation, the temperature difference creates a voltage signal which is proportional to the incident irradiation. These devices are spectrally almost unselective and measure the irradiation between 280 and 2800 nm. The parameters that influence the uncertainty of pyranometers are [22]:

- Irradiance level and spectral distribution of the solar radiation.
- Irradiance change rate during the measurement.
- Cosine effect.
- Ambient temperature.

- Pyranometer tilt angle.
- Pyranometer dome temperature.

The response time of pyranometers is in the range of 5-30s. Therefore, they react much slower than the PV modules on changing irradiance conditions. However, this effect is negligible in the monitoring of a utility scale PV plant.

Pyranometers are calibrated under indoor and outdoor conditions. The calibration uncertainties of experienced laboratories that calibrate according ISO 9846, ISO 9847 or equivalent, are in the range of 1-2% [23]. The expected daily uncertainty for pyranometers according to [24] is below 2% for secondary-standard pyranometers, below 5% for first-class pyranometers and below 10% for second-class pyranometers. According to [25] and [26] the overall uncertainty of the instantaneous irradiance measurement based on secondary standard pyranometers is approximately 3%.

Pyranometers are widely used in meteorological measurements and nearly all existing irradiation databases are validated on these measurements. With few exceptions [27] satellite derived irradiance data is compared with ground based pyranometers. This should be considered if the performance of a PV plant is compared with an initial energy yield assessment.

Crystalline silicon reference sensors

Crystalline silicon sensors have basically the same layout as the crystalline silicon PV modules of the plant. They are spectrally selective in the range of 400 nm to 1150 nm. The lower wavelength is determined by the transmission of the front glass and encapsulant whereas the longer wavelength is determined by the material's band gap. The response time of silicon sensors is in the millisecond range or below. The factors that influence the uncertainty of these sensors are mainly:

- Irradiance level.
- The angular distribution.
- Shift of transfer function over time (calibration drift).
- The ambient temperature.
- The temperature of the sensor.

Crystalline silicon reference sensors are calibrated under indoor and outdoor conditions. The calibration should comply with IEC 904-2 and -4 respectively. According to IEC 904-2, the calibration traceability of crystalline silicon sensors can be divided into:

- Primary reference devices.
- Secondary reference devices.
- Working reference devices [28] [29].

Crystalline silicon reference devices are used in order to estimate the STC power of a PV plant. This is completed when measuring IV curves of modules, strings or complete arrays in a PV plant. These devices are calibrated according to STC conditions (1000 W/m^2, 25°C and AM1.5 spectrum). Therefore they indicate the intensity of the equivalent AM1.5 spectrum, even though the instantaneous solar

spectrum is, most of the time, not identical to the AM1.5 spectrum. Assuming that the spectral response of the device is equal to that of the PV modules in the PV plant, the actual STC power of a PV plant can be estimated by extrapolating the instantaneous irradiance and module temperature to STC conditions. In cases where the spectral response is not equal, a spectral mismatch correction has to be undertaken.

On an annual basis, crystalline silicon sensors measure less irradiation than pyranometers. The highest absolute difference between the signal measured by a crystalline silicon sensor and a pyranometer is at clear sky conditions with a low diffuse/direct ratio [30]. The annual difference between the two sensor types depends very much on the sensor and the location. Recent publications [31], [32], [33] indicate that the deviation between different sensors installed in Germany varies considerably. On average, the annual irradiation measured by crystalline silicon sensors is 2-4% less than the irradiation measured by pyranometers. Hence, the annual *PR* of a PV plant in Germany that is calculated on the basis of crystalline silicon sensors may be on average 2 to 4% higher than the *PR* based on a pyranometer measurement. This has to be taken into account when comparing the *PR* of an operating PV plant with the *PR* estimated in the energy yield assessment. It should be mentioned that some publications propose a correction of the crystalline silicon sensor in order to convert it into a pyranometer signal and vice versa [34], [33]. However, these corrections are currently not widely applied in the PV community and their validation has not been carried out worldwide.

Table 4: Technical specifications of pyranometers and reference cells

Specification	Secondary standard [35]	First Class [35]	Second Class [35]	c-Si Reference cell
Response time	< 15 s	< 30 s	< 60 s	<< 1s
Non-stability	±0.8%	±1.5%	± 3%	± 0.2% [36]
Non-linearity	± 0.5%	± 1%	± 3%	< 0.5% [37]
Spectral selectivity	± 3%	± 5%	± 10%	c-Si:± 0.5% [38] high η: SMM=1.7% [39] a-Si: SMM=2.1% [40]
Tilt response	± 0.5%	± 2%	± 5%	up to 90%

In light of the points discussed above, the selection of the irradiance sensor depends on the purpose of the monitoring. Thermopile sensors are recommended where the performance of a PV plant is to be compared with performance figures as they are defined in the contracts that are based on an initial energy yield assessment. Silicon reference sensors are advantageous when verifying the PV plant's STC power or when checking the PV plant's response is in the per-second range, e.g., during scattered cloud conditions. In order to reduce the uncertainty of the measurement, either first class or secondary standard pyranometers or comparable crystalline sensors should be installed. In all cases it should be asked for a traceable calibration and the associated calibration certificate.
The sensor should be installed in a place were no near or far shading can affect the measurement, even if parts of the plant are affected by shading. Care has to

be taken to ensure that the sensor's orientation is exactly the same as the other modules. A slight error in the orientation of the sensor compared to the modules can derive a virtual time offset between the production measurements and the irradiation measurement. For large PV plants the installation of additional pyranometers is recommended. The signal of the sensors should be constantly compared in order to detect any malfunction.

The irradiance sensors should be checked and cleaned frequently. According to the location and season, an interval from 1 to 2 weeks is recommended. The sensors should be recalibrated in order to correct any bias in the measurement. If two sensors are installed and constantly compared, a recalibration every two years is reasonable and can be considered to comply with [41]. If only one sensor is installed, a yearly recalibration should be considered. During the recalibration the sensor should be replaced by a sensor of at least the same quality.

The use of satellite derived irradiance data may be an option for small scale PV plants where the cost of the irradiance sensor cannot be justified. A recent study shows quite good results for some providers of such data [42]. For shorter periods, satellite derived data has higher uncertainty and bias than calibrated sensors on site. When applied for computing the reference yield, the uncertainty of the data source should be watched in the same way as this is good practice for a sensor on site.

Energy monitoring

For electricity yield measurements, energy meters or true-rms power meters should be used. The inverter-integrated measurements are usually not sufficiently precise. Nevertheless, they may prove useful for identifying relative changes over time.

For more advanced monitoring the power or current on the junction box level or the string currents should be measured. The additional cost for advanced monitoring depends on the PV plant layout and capacity. The economic benefit of advanced monitoring compared to the simple inverter monitoring depends very much on the individual project. The economic benefit is higher when more energy is produced per installed power plant and results in a higher price per kWh. In case the PV plant produces less energy than expected, junction box or string based monitoring reduces the time and cost significantly for detecting the failure. If the PV plant is sold to a new owner, advanced monitoring gives more security about the quality of the plant. For these reasons, monitoring that registers the DC production at least on the junction box level is strongly recommended.

Some general recommendations for monitoring systems are:

- The availability of the monitoring data should be 99% or higher. Periods in which either data for irradiance or production is not available, should not be included in the analysis of the PV plant. A data availability of less than 95% indicates a low quality data acquisition system.
- The data should be sampled every second or faster. Averaged values should be stored every 5 to 15 minutes. Longer averages may hamper the analysis of the PV plant [43] whereas shorter intervals may overload the database.

2 Understanding Photovoltaic System Operation through Monitoring

2.1 Stamp Collections as Visual Tool

The broad variety of values that can be measured in a particular system has been illustrated in the previous section. At least plane-of-array irradiance (G_I) and AC power output P_{AC} are needed to calculate a *PR*, but very often various voltages, currents and temperatures are monitored, too (see Table 1 in sub-section 2.1). Especially for non-experts, the variety of the data and quite often the sheer amount of data can make it hard to proceed with a useful analysis.

The most straightforward way to rapidly gain first insights is to simply visualize the data as it was recorded, as a function of time. An example is given in Figure 1, depicting one week of G_I, module temperature T_{Mod}, P_{AC} and *PR*. These and the graphs shown in the following are dubbed "stamps", because their broad variety resembles the diversity of stamp collections.
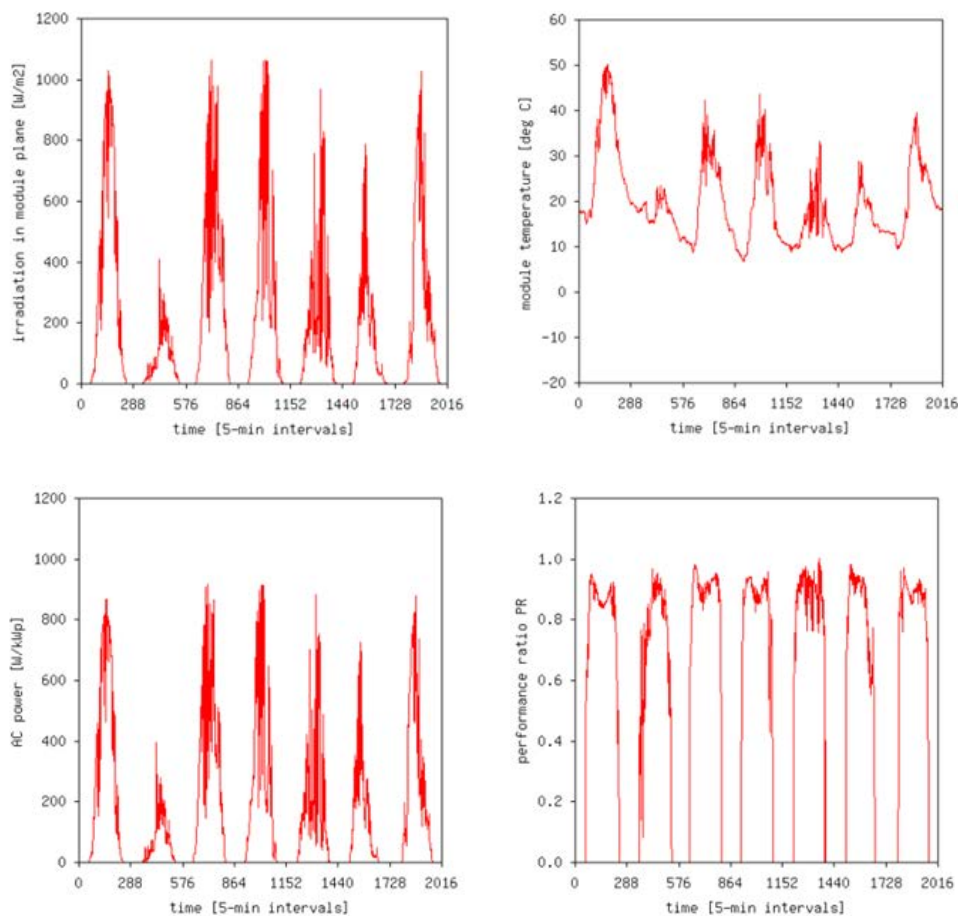

Figure 1: One week of basic monitoring data over time

The individual days of the one-week time sequence depicted in Figure 1 can still be distinguished for each "stamp-plot", due to the diurnal operation mode of PV power plants and zero-values for most quantities, or at least low values, such as for temperatures. For example one can easily recognize for the second day much lower irradiance and module temperature.

When looking at the detailed shape of the *PR* (bottom-right) one can also recognize a different shape during this second day as compared to the other days, which is formed like a "peak" rather than a "bath-tube". This well-known "bath-tube" shape of the *PR* during one entire day is caused by increased module temperatures. With negative temperature coefficients, an increase in module temperature causes a reduction of the *PR*. Consequently, the "bath-tub" shaped profile of the *PR* is well-pronounced on days with high module temperatures (top-right), which themselves are clearly related to irradiance intensity: obviously, modules will be warmer under high as compared with low irradiance intensity.

With many monitoring parameters being related to each other, it becomes clear that scatter plots of two parameters in 2-dimensional Cartesian coordinates can reveal much more information as compared with plotting data over time only. In the following, we illustrate and describe selected relationships depicted in Figure 2.

The two "stamps" in the first row of Figure 2 depict the AC vs. DC power (top-left), from which inverter efficiency can be calculated (top-right). When looking at inverter efficiency under low irradiation intensity, one can recognize that AC power output at very low irradiance becomes much lower than DC-power, due to the power consumption of the inverter itself, letting the efficiency drop. This cannot be recognized in the top-left plot because values are all very close to zero. Next, the two "stamps" in the second row of Figure 2 show the relation of module temperature with irradiance intensity, without (top-left) and with (top-right) ambient temperature factored in and in the bottom-left graph, the *PR* is plotted as a function of irradiation intensity. Finally, in the bottom-right "stamp" in Figure 2 the DC voltage (V_{DC}) as a function of module temperature is shown. As the pattern that can be recognized becomes difficult to explain, this "stamp" is shown in Figure 3 again as plot (a), together with only data from a summer week in (b), and finally also DC voltage as a function of in-plane irradiation in (c).

Figure 3a and Figure 3b both clearly show a horizontal line at 425 V, indicating that for many of the samples the system operates at the lower boundary of the inverter's maximum power point (MPP) tracking window. Moreover, plot (c) shows that this happens only at low solar irradiance. The focus on one week only allows identifying effects more sharply than for an entire year. Finally, plots (a) and (b) also point to a linear physical relationship, namely, the temperature dependence of the PV array voltage. Particularly the upper right points in (b) reflect this relationship while the lower-situated points hint towards inefficient operation points.
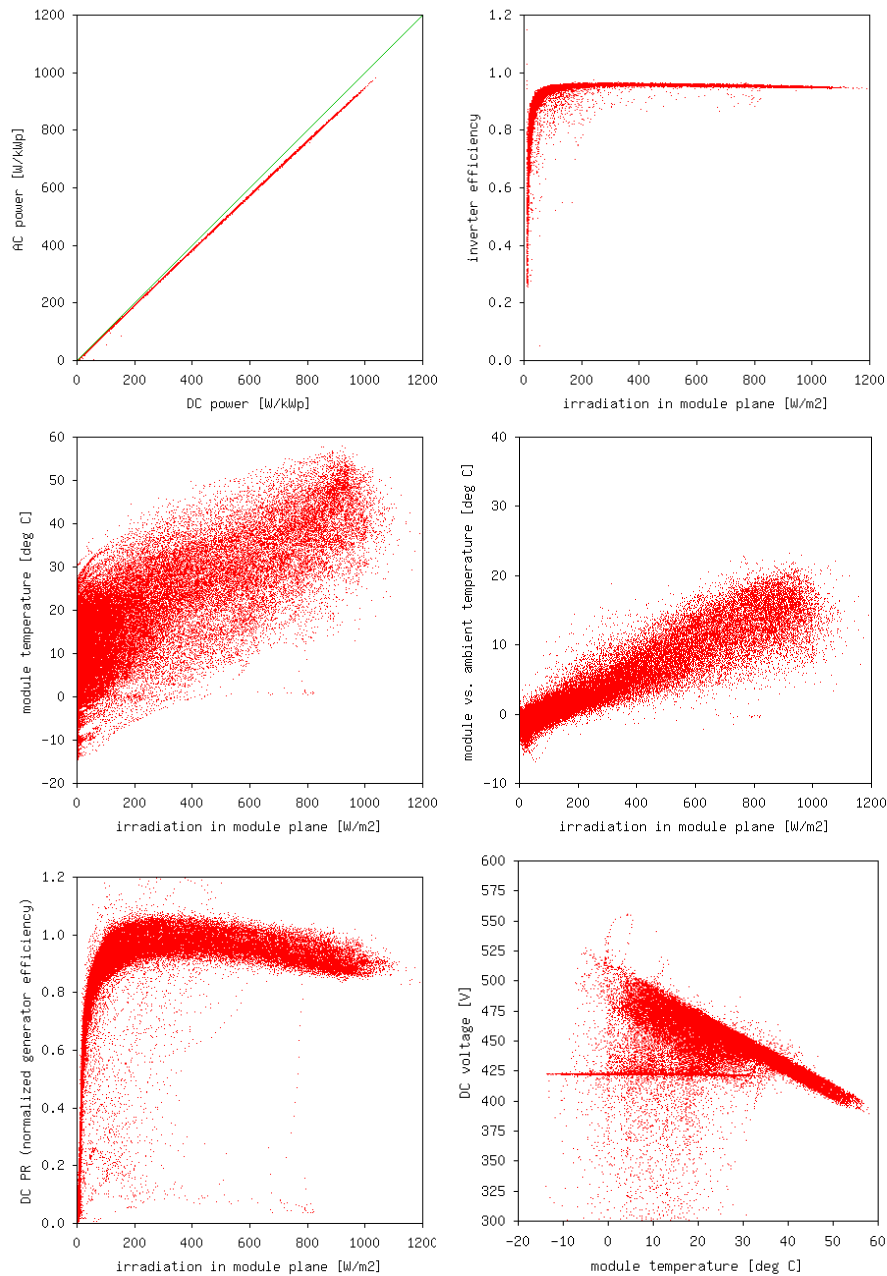
Figure 2: Selected relationships of monitoring data using annual 5-min datasets
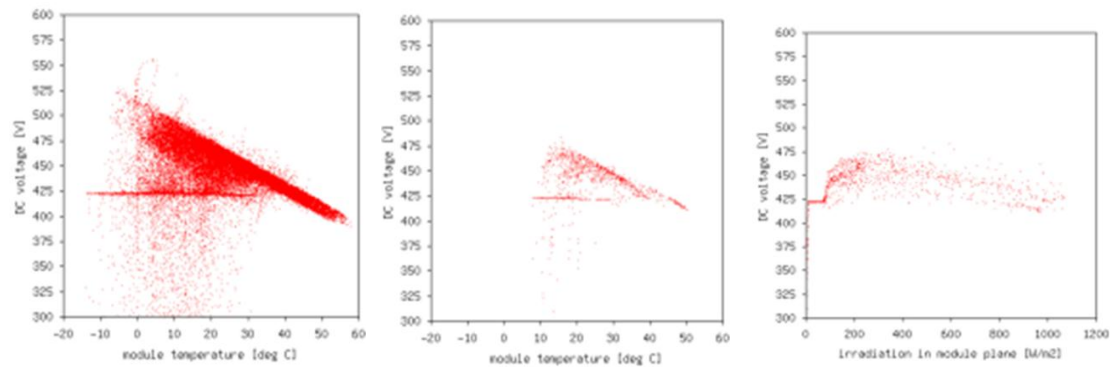
(a) V_{DC} vs T_{mod} (full year)　　(b) V_{DC} vs T_{mod} (summer)　　(c) V_{DC} vs $G_{\alpha,\beta}$ (summer)

Figure 3: Scatter plots of different PV system parameters for a full year (a) and a summer week around solstice (b and c); sampling period 5 min; system located in Germany, monitored by Fraunhofer ISE

11

Figure 4: Presenting "stamp plots" amongst Task 13 participants fostering exchange of expertise and deepening the understanding of PV performance aspects of a broader audience

Within the framework of Subtask 2 of the IEA PVPS Task 13, participants contributed "stamp collections" of PV performance data available to each individual participant. To this end, pre-defined sets of measured quantities were defined to be plotted and provided to all other task members. During some Task meetings, these "stamp collections" were shown to all participants, which proved very beneficial for exchanging ideas and expertise related to various PV performance phenomena (Figure 4). Figure 5 shows a sample of a "stamp collection" from one of these system.
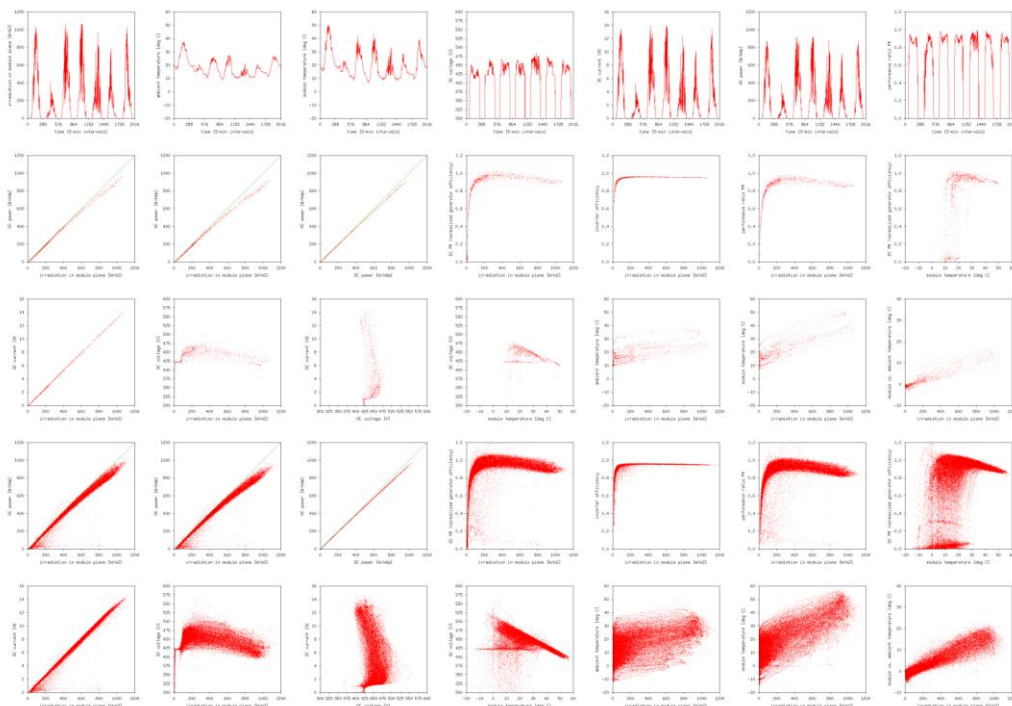
Figure 5: One "stamp collection" sample of one individual system.

2.2 Guidelines for Interpretation of Monitoring Data

In this section we introduce, illustrate and discuss the method of periodic linear regression. This method was developed by 3E and has first been published in [44]. It departs from a limited collection of plots along with interpretation guidelines for the analysis of PV monitoring data. The plots are based on simplified physical relationships and allow for deriving linear model parameters from regression. Updated periodically, such regression-based linear models allow for following the operational properties of the system and its components over time using a mathematical methodology. The selection presented here covers the full energy conversion chain as illustrated in Figure 6. Notably, for the classical yield and loss quantities, here we use small letters when referring to instantaneous values or averages over a short recording period. The plots may serve for identifying and interpreting common design flaws and operational problems or simply for documenting the proper operation of the installation. The data sources are listed in Annex A.

We intentionally do not introduce more sophisticated models as they are used for scientific evaluation or implemented in PV modeling software. For such models we refer to the PV Performance Modeling Collaborative [45] that provides a large documentation of models for PV.

Figure 6: Energy flow in a grid-connected photovoltaic system

2.2.1 Approach

PV System Parameters

Figure 6 illustrates the energy flow in a grid-connected photovoltaic system with a limited but selected collection of variables describing the main energy conversion steps taking place within the system. The variables shown in Figure 6 are briefly defined in Annex B.

Application

In practice, the plots should serve for identifying a simplified physical relationship between two variables. The variables are measured or can ea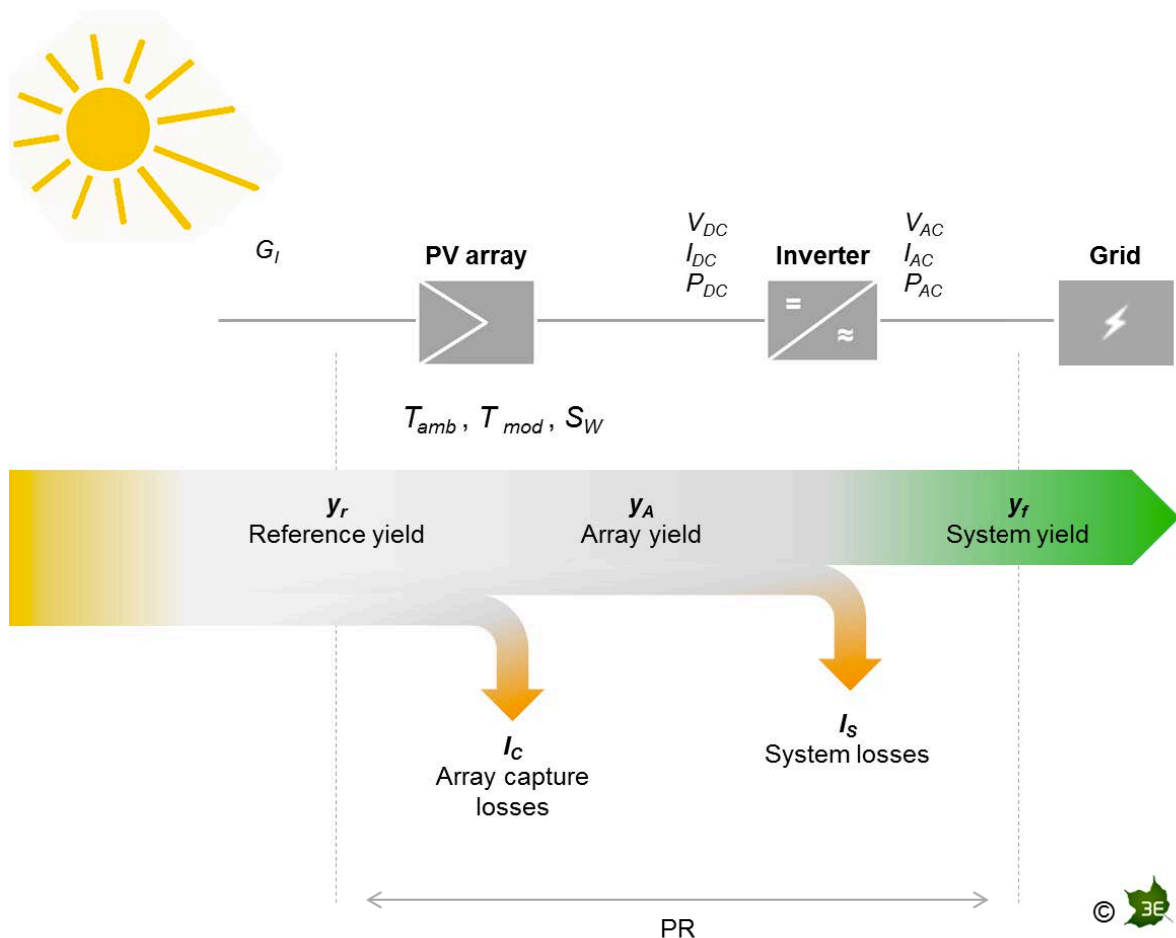sily be derived from measured variables. This method assumes that the relationship being used remains constant over time.

Such a physical relationship can then be approximated as a straight line by means of linear regression. The thus identified linear relationship may be considered characteristic for the energy conversion step to be monitored. In the practical application, this relationship can be identified periodically: recent samples or regression lines may be compared to historical lines and updated periodically in order to identify trends or sudden changes.

This application yields several indicators for the operation of the different energy conversion steps or sub-systems:

- regression lines not changing significantly over time indicate that the system properties remained constant;
- changing regression lines over time indicate a trend-wise change of system parameters;
- samples suddenly significantly deviating from the regression lines hint towards exceptional operating points;
- samples regularly deviating from the regression lines hint towards a design flaw.

Notably, these indicators may hint towards design flaws or failure by flagging inconsistent operating conditions. However, strictly speaking, no firm conclusions on the cause of irregular operation can be drawn from this analysis only. In practical application these indicators should be checked on their statistical significance by, e.g., performing a residual analysis. If they are significant, more detailed checks including a site visit would probably be launched.

Selection of Relationships and Plots

A limited number of simplified relationships and plots can be selected for analysis of the measured data (see Figure 7). The level of detail into which the PV monitoring data are analyzed depends on the required purpose. In practice it also depends on the available data and the effort considered reasonable for the purpose.

When only the PV power to the utility grid and the in-plane solar irradiance are available, the performance can be followed on the system level. If available,

module temperature is the most useful complement here. This is indicated in the upper row of Figure 7.

The middle row shows plots, recommended for a more specific analysis of different conversion steps, namely, the thermal behavior of the module, the performance on array level rather than on system level and the resilience of the utility grid voltage on active power injected at the connection point.

Finally, the third row shows relationships that reflect specific or secondary relationships: the most important one is the array voltage versus module temperature. Any effects that manifest themselves between PV array and inverter would lead to DC voltage deviating from the linear voltage-temperature behavior. Moreover, this row also shows how to take into account secondary effects as, e.g., wind speed.

In the following sections we present these relationships and the respective plots of measured data for all relationships listed in Figure 7. We discuss their application and illustrate how they can serve to distinguish flaws and failures from proper operation with examples from many different IEA PVPS member countries.
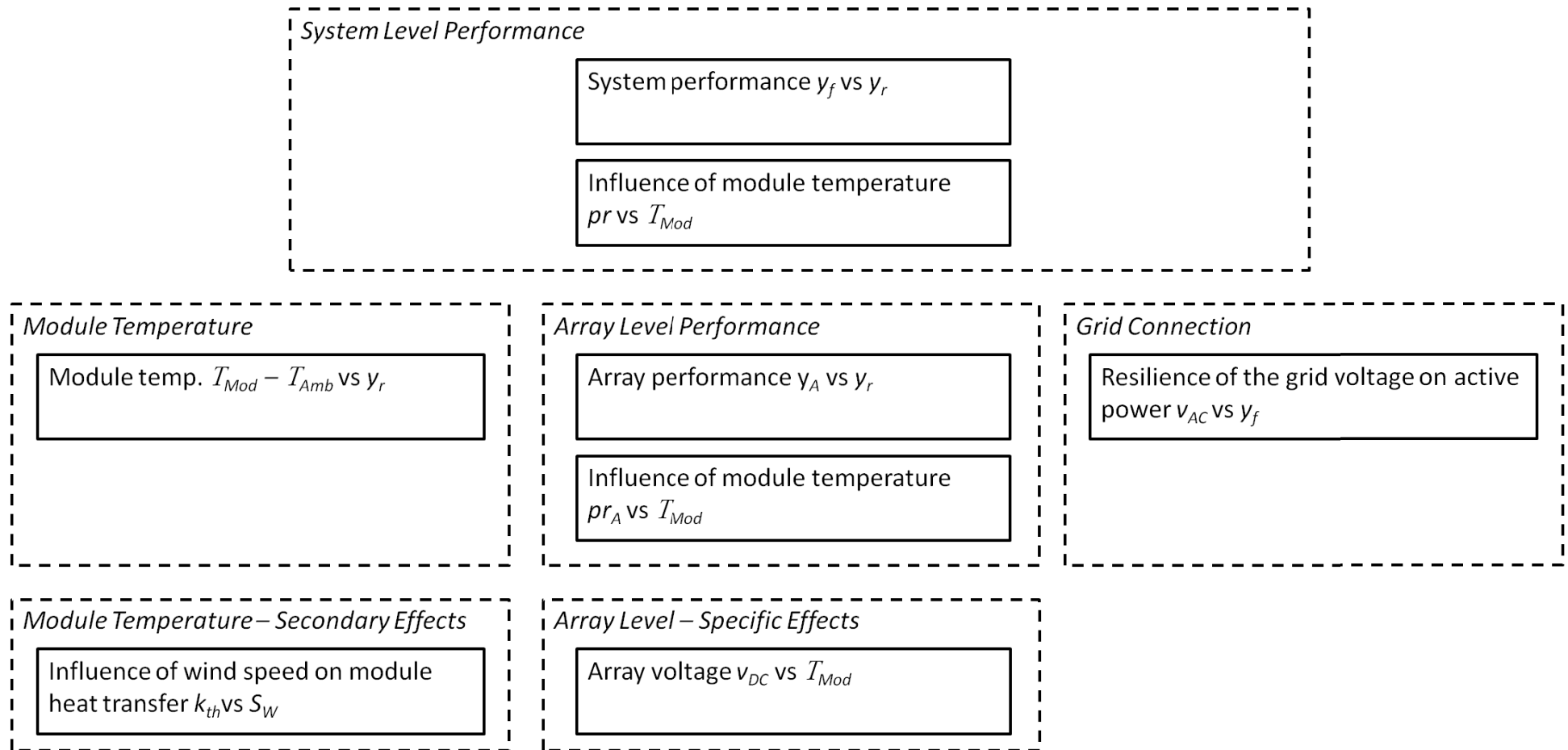
Figure 7: Overview of first-order relationships for the description of PV systems and components with monitoring data

2.2.2 Photovoltaic System Performance

Analytical Description

System yield versus reference yield is the most general set of performance parameters for a grid-connected PV system. This relationship represents the overall efficiency of energy conversion. The required variables power to utility grid and in-plane irradiance are always the first to be monitored.

As a very first approximation, the PV system may be considered linear. With this assumption, the system yield is proportional to the reference yield. When measurements of system yield are plotted over reference yield, their relationship can be approximated by a straight line through the origin. This line can be determined by linear regression throughout all data samples. Its slope $\overline{pr}$ approximates the average performance ratio over all samples.

As a first-order PV system model, the system can then be described analytically as

$$y_f = \overline{pr}\ y_r, \tag{1}$$

with
$\overline{pr}$ the average performance ratio,
y_f the instantaneous system yield and
y_r the instantaneous reference yield.

Plotting the scatter plot with a new regression line for each week (Figure 8) allows identifying the slope and, hence, the average performance ratio per week. Consequently, sudden changes from week to week as well as significant trends are indicated by the change of the slope.

Examples and Interpretation

The PV installation presented in Figure 8 suffered from shadowing by vegetation on the array. Figure 8a shows data from the installation in proper operation, after the vegetation had been cut: for four subsequent weeks the weekly $\overline{pr}$ is varying only slightly. These slight variations are normal and may be due to changing ambient and module temperature. Figure 8b shows data from the same installation during the previous four weeks before the vegetation was cut: the weekly $\overline{pr}$ was decreasing from week to week.

The PV installation presented in Figure 9 was operating normally until the first week of May 2012. In March 2012, the four weekly regression lines are close. From week 2 of May 2012 onwards, the slope of the regression line is consistently lower. Notably, the line for week 2 in May does not match the underlying samples. This is due to a sudden change occurring in the course of this week. Some values match the line of week 1 and the others ones of week 3 and week 4. As a result the regression line of week 2 lies in between. This sudden reduction in $\overline{pr}$ is due to the failure of one of the three inverters in the installation.
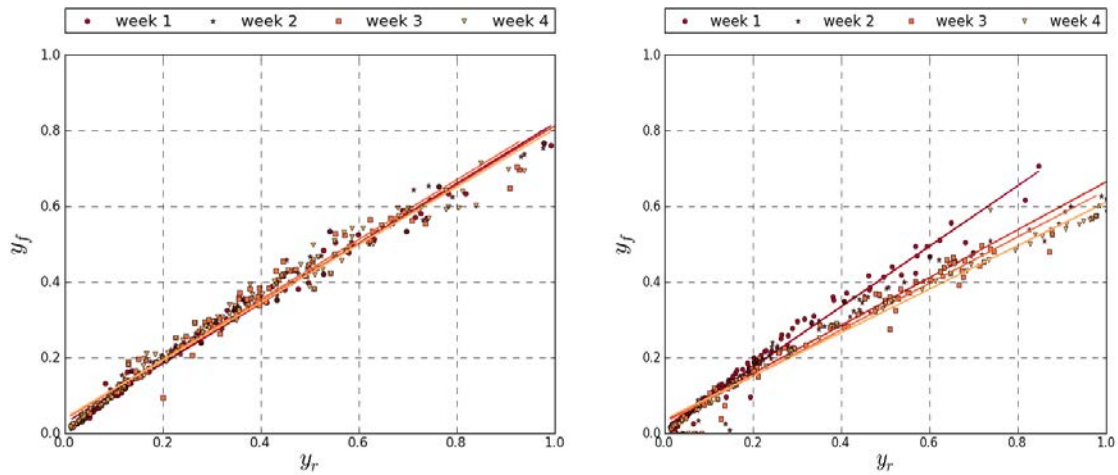
(a) Not shadowed – June 2012   (b) Shadowed by vegetation – May 2012

Figure 8: System yield (y_f) versus reference yield (y_r) for hourly averages from BE1 (see Annex A); different subsequent weeks in June and May 2012
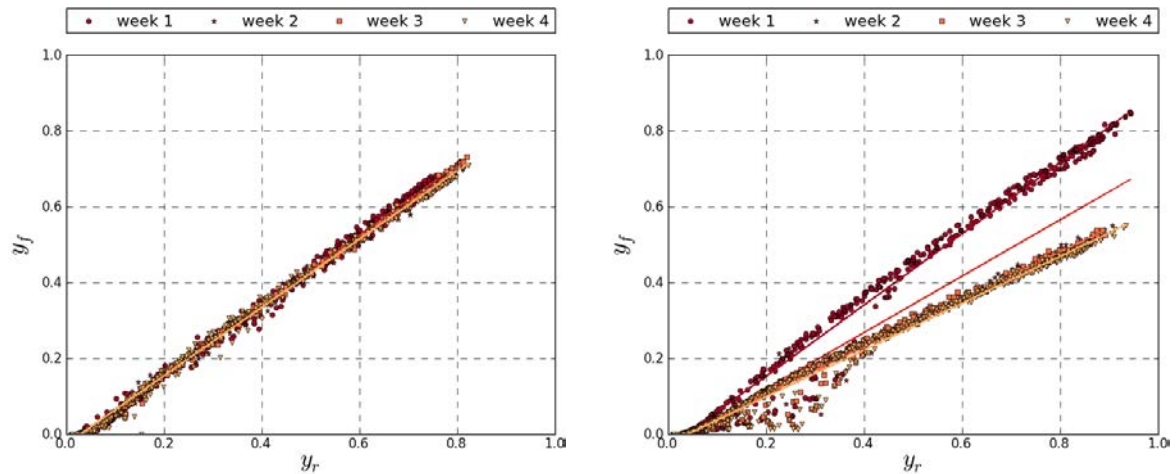
(a) Normal operation – March 2012   (b) Inverter failure (1/3) – May 2012

Figure 9: System yield (y_f) versus reference yield (y_r) for 15-min averages from SE1 (see Annex A); different subsequent weeks in March and May 2012

Figure 10 shows a similar case as Figure 9. The installation was operating normally until end of October (week 2 in Figure 10b) when one out of two strings connected to the inverter got interrupted. In the subsequent weeks the slope of the regression lines is reduced by half. In contrast to the data for Figure 9, here the entire period during which the fault persisted was characterized by relatively low irradiance with y_r values all below 0.5.

18
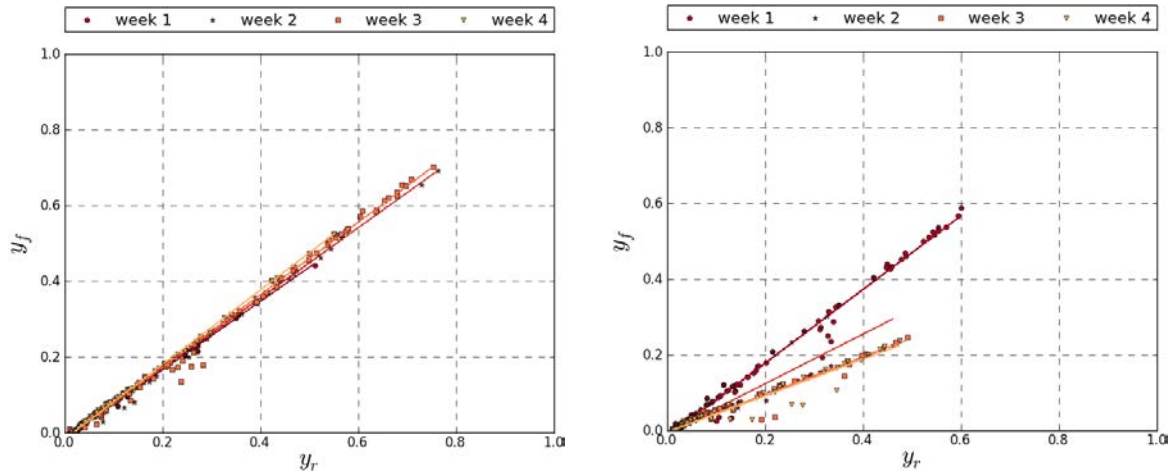
(a) Normal operation – 21/09-19/10/2012   (b) String fault – 21/10-18/11/2012

Figure 10: System yield (y_f) versus reference yield (y_r) for hourly averages from NO1 (see Annex A); different subsequent weeks from September to November 2012

Practical Use

The relationship between system yield and reference yield stands for the overall conversion efficiency of the installation. It is based on two measurements only and it can reflect all kinds of phenomena during the operation of a PV system.

Phenomena we have seen are:
- Shading.
- Defective strings or inverters.
- Potential-induced degradation (PID).
- Power limitation (inverter under sizing).

However, the scatter can be relatively wide and smaller disturbances will often not appear to be statistically significant. Especially variations in module temperature will cause deviations from the regression line during normal operation. Moreover, this relationship alone does often not easily allow for conclusions of the type of the design flaw or disturbance.

2.2.3 Influence of Module Temperature on System Level

Analytical Description

Photovoltaic module temperature is the most significant parameter affecting the PV system performance. The instantaneous performance ratio can be considered a linear function of module temperature [4]. When only the overall system *pr* is available, the system behavior can then be described analytically as

$$pr = pr_0 \, (1 + \gamma \, \varDelta T), \tag{2}$$

with
$\varDelta T$ $T_{mod} - T_{STC}$ the difference to 25 °C under standard testing conditions,
γ the temperature coefficient of power over the measured range of irradiance (usually negative),
pr   the instantaneous performance ratio,
pr_0 the model performance ratio at 25 °C.

If the module temperature is measured in addition to in-plane irradiance and power to the utility grid, the coefficients γ and pr_0 can be determined by linear regression. In practice this works well for high irradiance levels and we recommend omitting the samples measured at low irradiance from the regression, i.e., with $G_l < 600$ W/m^2. When pr values based on measurements are plotted over the module temperature, their relationship can be approximated by a straight line. Its slope can be interpreted as temperature coefficient of the PV array's output power.

Notably, if this analysis is based on power to the utility grid, the regression also accounts for any thermal effects and losses taking place in the inverter. Therefore, we recommend using the array performance ratio based on array power instead (see following sections). However, if no array or string level measurements are taken at the PV array, this approach can already yield good analytic insight in the array and system performance.
Plotting the scatter plot with a new regression line for each week (Figure 11) allows identifying the slope and intercept per week. Both values are expected to remain approximately constant over time. Consequently, sudden changes in these parameters from week to week would hint at acute disturbances. A significant trend over several weeks would hint towards a gradual change in system performance.

Examples and Interpretation

Figure 11 shows the plot of performance ratio as a function of module temperature for the same installation and data set as Figure 9. Here, the inverter failure has caused a reduction of pr by one third that is indicated in Figure 11b by a parallel shift of the regression lines towards lower intercept values. For week 2, the recorded samples are situated either on the line for week 1 (normal operation) or on the lines for weeks 3 and 4 (inverter failure). As a consequence, regression through the points of week 2 returns a line that is situated somewhere in the middle.
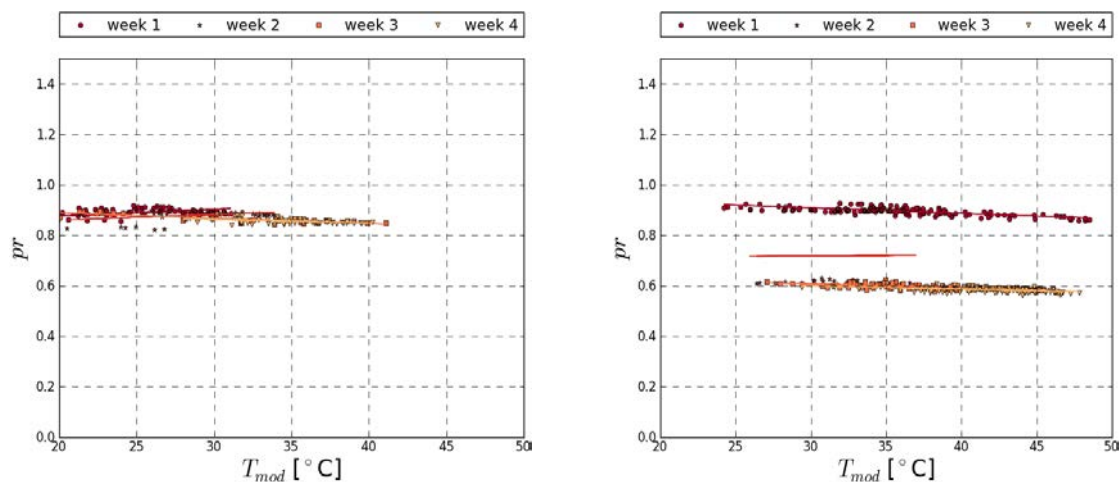
(a) Normal operation – March 2012   (b) Inverter failure (1/3) – May 2012

Figure 11: Performance ratio (pr) versus module temperature (T_{mod}) for 15-min averages from SE1 (see Annex A) (samples with $G_l > 600$ W/m^2); different subsequent weeks in March and May 2012

As with system yield versus reference yield, the relationship of performance ratio over module temperature reflects the common phenomena during the operation of a PV system. However, here the module temperature is specified and, hence, this view complements the previous one with this additional parameter.

Phenomena we have seen are:
- Shading.
- Defective strings or inverters.
- Potential-induced degradation (PID).
- Power limitation (inverter under sizing).

However, smaller disturbances will often not appear to be statistically significant. In particular variations in module temperature will cause deviations from the regression line during normal operation. Moreover, this relationship alone does often not easily allow for conclusions of the type of the design flaw or disturbance.

2.2.4 Photovoltaic Array Performance

Analytical Description

The PV array performance is firstly reflected by the relationship of array yield versus reference yield. In contrast to the one of system yield versus reference yield, this relationship isolates the array from the rest of the system (assuming ideal MPP tracking). In practice it can be treated the same way as the system yield. Obviously, this analysis requires the measurement of PV array output power.

As a very first approximation, the PV array may be considered linear. With this assumption, the array yield is proportional to the reference yield. When measurements of array yield are plotted over reference yield, their relationship can be approximated by a straight line through the origin. This line can be determined by linear regression throughout all data samples. Its slope $\overline{pr_A}$ approximates the average array performance ratio over all samples.

As a first-order PV array model, the array can then be described analytically as

$$y_A = \overline{pr_A} \; y_r, \tag{3}$$

with
$\overline{pr_A}$ the average array performance ratio,
y_A the instantaneous array yield and
y_r the instantaneous reference yield.

As with the relationship of system yield versus reference yield introduced in Section 2.2.2, plotting the scatter plot with a new regression line for each week allows identifying the slope and, hence, the average array performance ratio per week. Consequently, sudden changes from week to week as well as significant trends are indicated by the change of the slope.

Examples and Interpretation

Figure 12 shows plots of PV array performance and PV system performance for the same PV installation and time period.

(a) PV array performance   (b) PV system performance
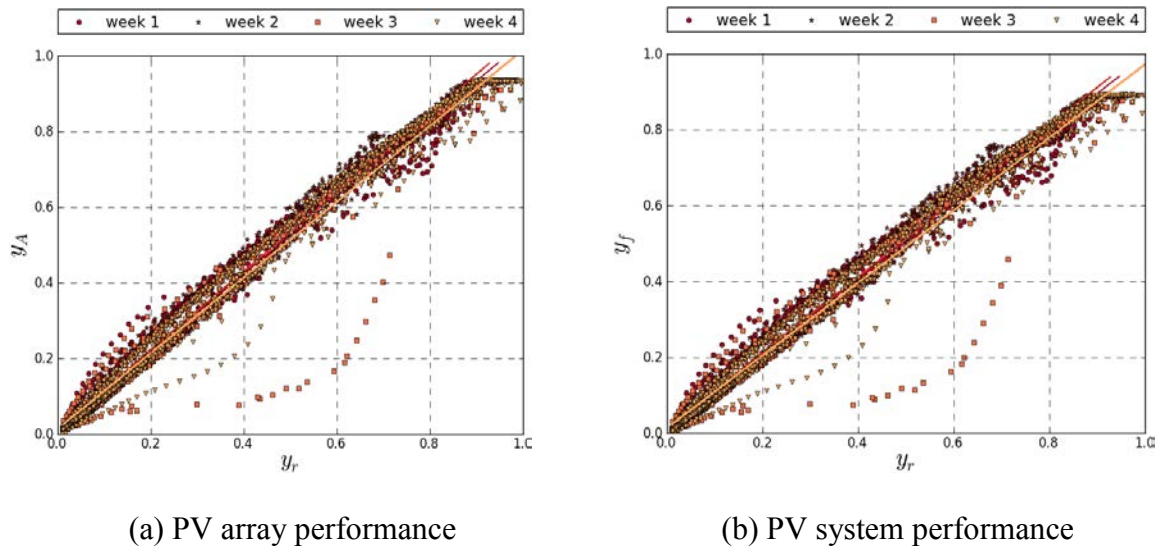
Figure 12: Plots of PV array yield (y_A) and system yield (y_f) versus reference yield (y_r) for 5 minute averages from SE2 (see Annex A) (inverter 1 only); different subsequent weeks in March 2011

The scatter lines in Figure 12a) and b) at first sight have similar shapes with larger slopes in Figure 12a). Physically, system yield and array yield differ in terms of system losses only. Their ratio for a given sample equals the inverter efficiency while the sample was taken. Moreover, in both plots, the ordinate is capped for reference yields above approximately 0.88. This power limitation indicates inverter undersizing as it has been common practice in Northern Europe for many years.

For all weekly regression lines, the slope varies around one. Such values for the measured average performance ratio appear to be relatively high even for instantaneous values. The reason for this is unknown. Factors influencing the performance ratio are the module temperature, but also the solar spectrum, the device used for measuring in-plane irradiance and the precision of the nominal power of the plant used for normalization.

Practical Use

The relationship between array yield and reference yield stands for the conversion efficiency of the PV array. It requires the measurement of PV array output power. First of all it reflects the same phenomena as the relationship of system yield versus reference yield. Secondly, if P_{AC} and P_{DC} have been measured precisely and with high time resolution, the comparison of both relationships allows for splitting losses into capture losses (L_C) and system losses (L_S) as illustrated in Figure 6.

Notably, with this approach, only those losses which cause a physical dissipation of power in the inverter will be allocated as system losses. Phenomena that are caused by the inverter but manifested somewhere else will be equally visible in both relationships. Examples would be a poor performance of the inverter's MPP tracker or the limitation of output power as seen in this example.

2.2.5 Influence of Module Temperature on Array Level

Analytical Description

As for the PV system level, also the instantaneous array performance ratio (pr_A) can be considered a linear function of module temperature. Like for the yield values in Section 2.2.4, it isolates the capture losses from the system losses as they occur in the inverter. If the array power is measured, this approach is preferred because the resulting temperature coefficient γ also physically represents the temperature coefficient of the PV array. The array behavior can then be described analytically as

$$pr_A = pr_{A,0}\,(1 + \gamma\,\Delta T), \tag{4}$$

with

ΔT $T_{mod} - T_{STC}$ the module temperature above 25 °C standard test conditions,
γ the temperature coefficient of power (usually negative),
pr_A the instantaneous array performance ratio and
$pr_{A,0}$ the model array performance ratio at 25 °C.

If the module temperature is measured in addition to in-plane irradiance and PV array output power, the coefficients γ and $pr_{A,0}$ can be determined by linear regression. In practice this works well for high irradiance levels and we recommend omitting the samples measured at low irradiance from the regression, i.e., with $G_I < 600$ W/m^2. When pr_A values based on measurements are plotted over the module temperature, their relationship can be approximated by a straight line. Its slope can be interpreted as temperature coefficient of the PV array's output power.

Plotting the scatter plot with a new regression line for each week (Figure 13) allows identifying the slope and intercept per week. Both values are expected to remain approximately constant over time. Consequently, sudden changes in these parameters from week to week would hint at acute disturbances. A significant trend over several weeks would hint towards a gradual change in system performance.

Examples and Interpretation

Figure 13 shows plots of array performance ratio versus module temperature for one PV system in different situations. Figure 13a is based on the same data set as Figure 12. The slopes and intersects of the regression lines are the same for weeks 1, 2 and 4. For week 3, the line is completely different and contrasting with the physical understanding that, for crystalline PV modules, the array efficiency decreases with increasing temperature. The reason for the exceptionally low pr_A values at low temperatures as they occur in this week could be snow on the PV array while the radiation sensor was free. In Figure 13b no such exceptional behavior is visible. Although the scatter clouds are relatively wide in terms of pr_A, all regression lines are close to each other. Notably, the review of data from several years and installations has shown many inconsistencies of the kind seen in Figure 13a especially during the winter months.
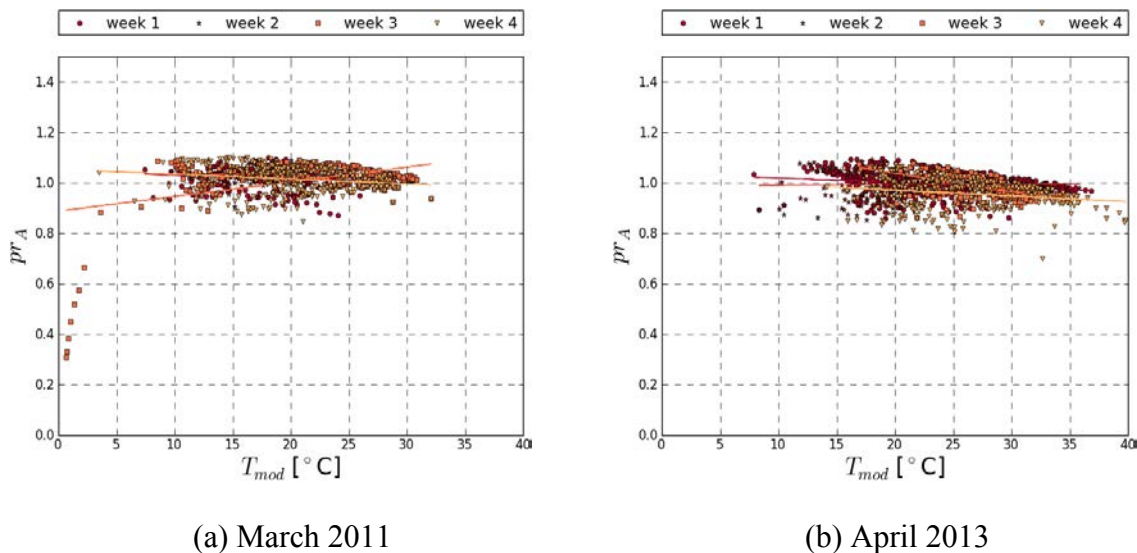
<center>(a) March 2011   (b) April 2013</center>

Figure 13: Array performance ratio (pr_A) versus module temperature (T_{mod}) for 5 minute averages from SE2 (see Annex A) (inverter 1, samples with $G_I > 600$ W/m^2); different subsequent weeks in March 2011 and April 2013

The combined use of array yield versus reference yield and array performance ratio versus module temperature is illustrated in Figure 14 for two different installations in Malaysia.

For each of the four plots, the regression lines for the different weeks are virtually identical; hence, the system operation is stable over the four weeks. Comparing the amorphous silicon installation (a and b) with the crystalline silicon installation (c and d) reveals a significantly larger scatter for crystalline silicon. The array performance ratio (pr_A) is relatively low for the crystalline silicon plant. The influence of module temperature on the array performance ratio is much stronger for crystalline silicon than for the amorphous silicon plant. This is immediately visible when comparing Figure 14b) and d) and it also explains why in Figure 14c the scatter of y_A versus y_r bends to the right for high y_r values.

Practical Use

As for performance ratio, the relationship of array performance ratio versus module temperature describes the thermal behavior of the PV array. And it complements the relationship of array yield versus reference yield with module temperature as additional parameter. Together both relationships can be used to determine a high-level parametric model of the PV array as they are typically used for power forecasting or the calculation of expected yield. Moreover, since they reflect physical relationships, any changes in their parameters point towards a change in the underlying physical reality, e.g., degradation, a fault, snow or shadow.

Altogether, the previous examples show how already with two linear relationships based on three data sets, the PV array can be described distinctively even for relatively short periods. The analysis may be sophisticated further. For example, if the behavior at low irradiance is of particular interest, non-linear terms of reference yield could be added. However, in line with the objectives of the present report, no such models will be treated here. Instead, in the following subsections, the same linear approach will be applied in order to include further parameters.

<center>24</center>

(a) a-Si, y_A vs y_r (MY1)

(b) a-Si, pr_A vs T_{mod} (MY1)

(c) c-Si, y_A vs y_r (MY2)

(d) c-Si, pr_A vs T_{mod} (MY2)
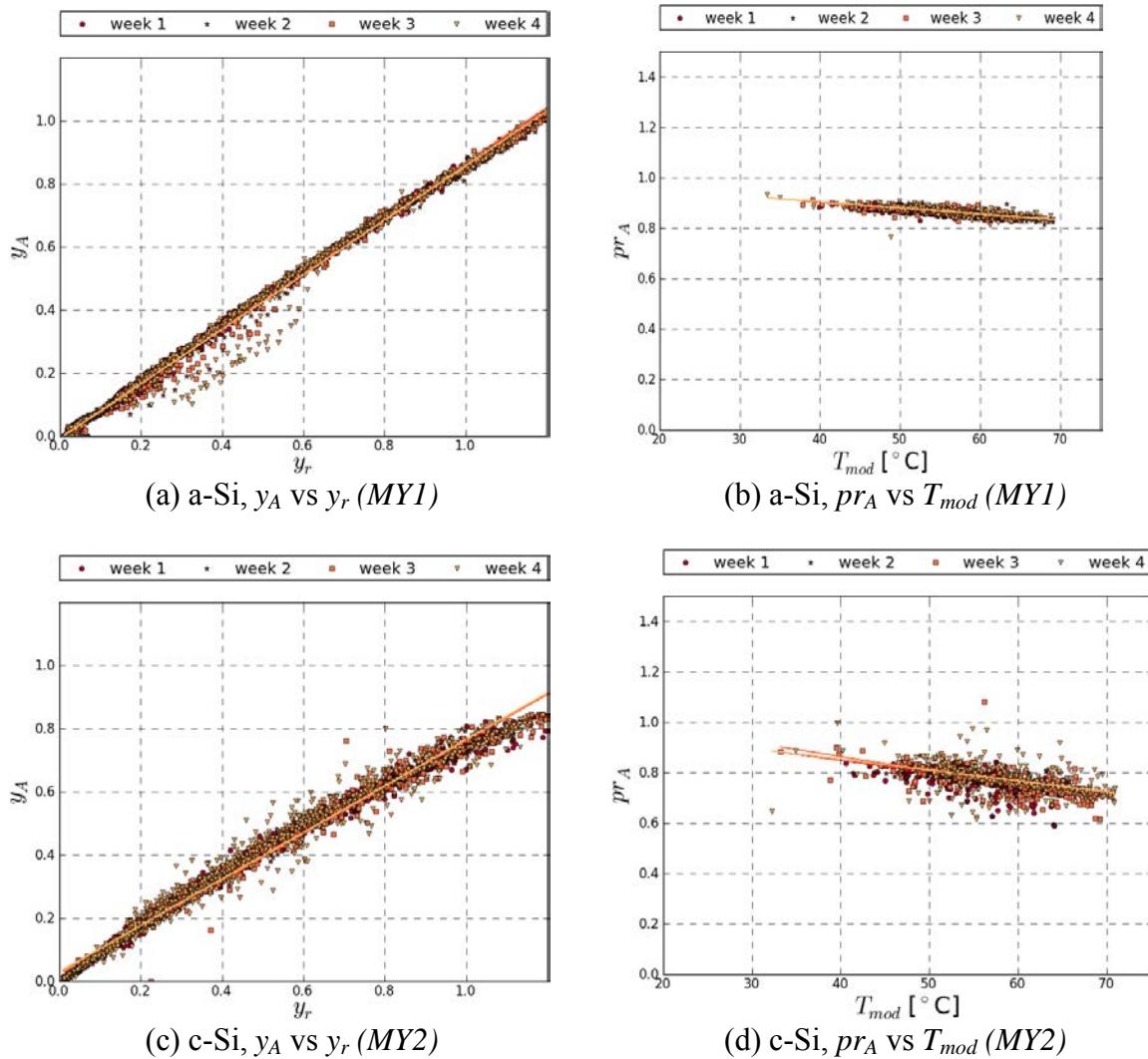
Figure 14: Array yield and array performance ratio for two installations at the same site MY1 and MY2 with 5-min averages (see Annex A); four subsequent weeks in October 2012

2.2.6 Module Temperature

Analytical Description

The temperature of a PV module follows from its heat balance. As a linear approximation and neglecting the thermal capacitance of the module, the heat dissipated to the environment is proportional to the solar radiation received by the module. Moreover, the heat dissipated is proportional to the difference between module and ambient temperature. Consequently, the relationship between this temperature difference and the instantaneous reference yield can be approximated by a straight line. The slope of this line k_{th} can be interpreted as equivalent thermal resistance over all data samples. Typical values of equivalent thermal resistance k_{th} for a PV array range around 0.027 to 0.032 K/(W/m^2) [15], [46].

25

Hence

$$T_{mod} - T_{amb} = k_{th} \, y_r, \qquad\qquad (5)$$

with
T_{mod} the module temperature,
T_{amb} the ambient temperature,
y_r the instantaneous reference yield and
k_{th} the equivalent thermal resistance.

Notably, in physical terms, a fraction of the in-plane irradiance is reflected while another fraction is converted into electricity and only the rest is dissipated as heat within the PV array. This heat is then flowing to the environment through conduction, convection and radiation. Consequently, k_{th} is not strictly a thermal resistance but it comprises all mechanisms of heat transfer and it also figures in the effects of reflection and PV power generation.

Plotting the temperature difference $T_{mod} - T_{amb}$ against y_r with a new regression line for each week, allows identifying weekly k_{th} values for all samples involved. As long as the physical set up of the PV array does not change, this value should not significantly change either. As a result, sudden changes from week to week as well as significant trends are indicated by changes in the slope of the weekly regression lines.

Examples and Interpretation
Figure 15 and Figure 16 show the temperature difference $T_{mod} - T_{amb}$ versus y_r for measured data. The scatter clouds for this relationship are generally much more dispersed than for the relationships discussed before. However, when comparing the slopes of the regression lines week per week, these are consistently close.

For the installation in Italy, the lines are somewhat steeper in late spring (Figure 15b) than in winter (Figure 15a). Remarkably, weeks 1 and 4 in Figure 15a show a lot of very low samples far below their regression lines. These may be related to high wind speed and will be discussed in the following section.

For the installation in Norway, weeks 1 and 2 of Figure 16a, the slope of the regression line is unexpectedly low with k_{th} around 0.015 K/(W/m^2) in week 1. This is not due to exceptional cooling but to a detachment of the temperature sensor from the array's back surface. This fault was corrected in the course of week 2. On the contrary, the somewhat lower slope of week 3 as compared to week 4 is correlated with higher wind speed values in week 3.
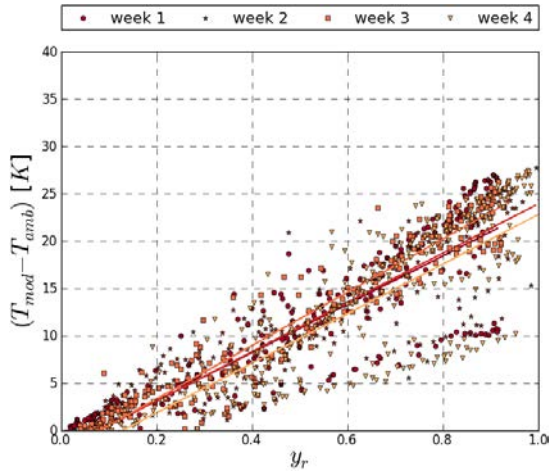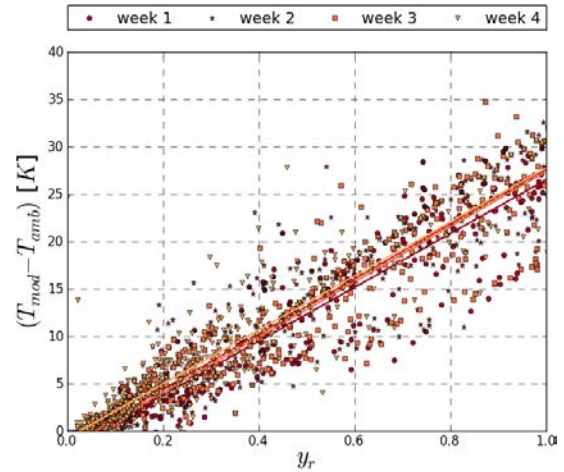
(a) Winter – 15/02-14/03/2012   (b) Late spring – 15/05-12/06/2012

Figure 15: Temperature difference ($T_{mod} - T_{amb}$) versus reference yield (y_t) for 15 minute averages from IT1 (see Annex A); different subsequent weeks in February/March and May/June 2012
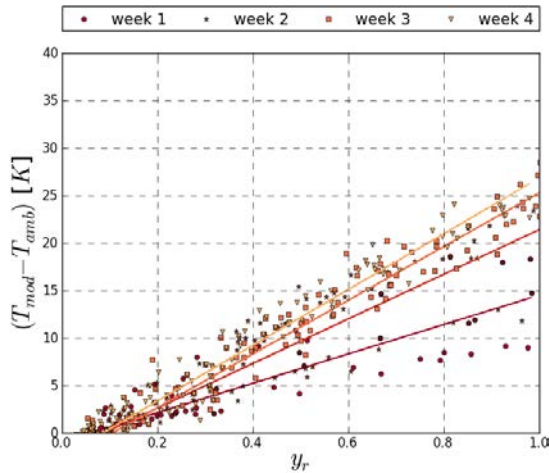
(a) Sensor detachment – July 2012   (b) Normal operation – August 2012
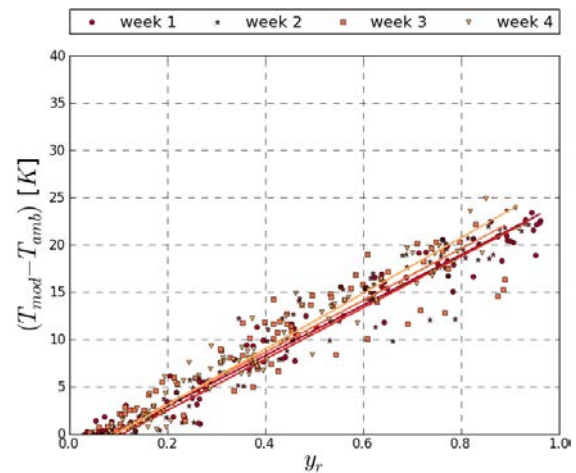
Figure 16: Temperature difference ($T_{mod} - T_{amb}$) versus reference yield (y_t) for 15 minute averages from NO2 (see Annex A); different subsequent weeks in July and August 2012

Practical Use

The temperature behavior of the PV array as a function of irradiance reflects how well the PV modules can conduct heat and how well the installation is ventilated. Therefore, the equivalent thermal resistance can be monitored in order to supervise the thermal situation.

Exceptionally high module temperature occurs when the PV array is not well ventilated. An increase in equivalent thermal resistance would mean that the installation is not anymore ventilated as before, e.g., by material accumulating in the gap between its backside and the roof. High module temperature can also occur punctually at some modules or cells in case of local module or cell failures, e.g., hot spots. A decrease in equivalent thermal resistance could point towards a situation where the PV module carrying the temperature sensor is shadowed. But

in several cases observed, the irregular thermal behavior simply was caused by a detached module temperature sensor.

2.2.7 Module Temperature and the Influence of Wind Speed

Analytical Description

Under real operating conditions, module temperature is not only proportional to the ambient temperature and in-plane irradiance, but it also depends on the wind speed, wind direction and relative humidity. Depending on different secondary effects as, e.g., the system assembly and installation conditions, the equivalent thermal resistance of the heat transfer can be influenced to a greater or lesser extent by the wind speed.

Complementing the first approximation above (Section 2.2.6), now wind speed is taken into account. The equivalent thermal resistance can be approximated by an exponential function of wind speed [47],[48]. In other words

$$k_{th} = k_{th,0} \; e^{-C_{th} S_W} ,$$ (6)

with
k_{th} the equivalent thermal resistance,
$k_{th,0}$ the equivalent thermal resistance without wind,
C_{th} coefficient for thermal convection and
S_W wind speed.

The variable k_{th} represents the equivalent thermal resistance for a given sample defined in equation 5. Plotting it on a semi-logarithmic scale versus S_W with a new regression line for each week allows determining the parameters $k_{th,0}$ and C_{th}. As a result, sudden changes from week to week as well as significant trends are indicated by changes in the slope of the weekly regression lines.

Examples and Interpretation

Figure 17 shows the equivalent thermal resistance versus wind speed for the same data set as used for Figure 15. In winter and in late spring, the weekly regression lines differ only little in slope and intercept. In Figure 17a we can identify a large cluster of points for low wind speeds in the range of 0.5 to 2 m/s and a smaller one around 4 to 7 m/s, where mainly data points from week 1 and week 4 can be found. These data points at higher wind speed correlate with a lower equivalent thermal resistance. This is in line with the observations made before with regard to Figure 15a and can serve to explain the partly lower equivalent thermal resistance observed there.
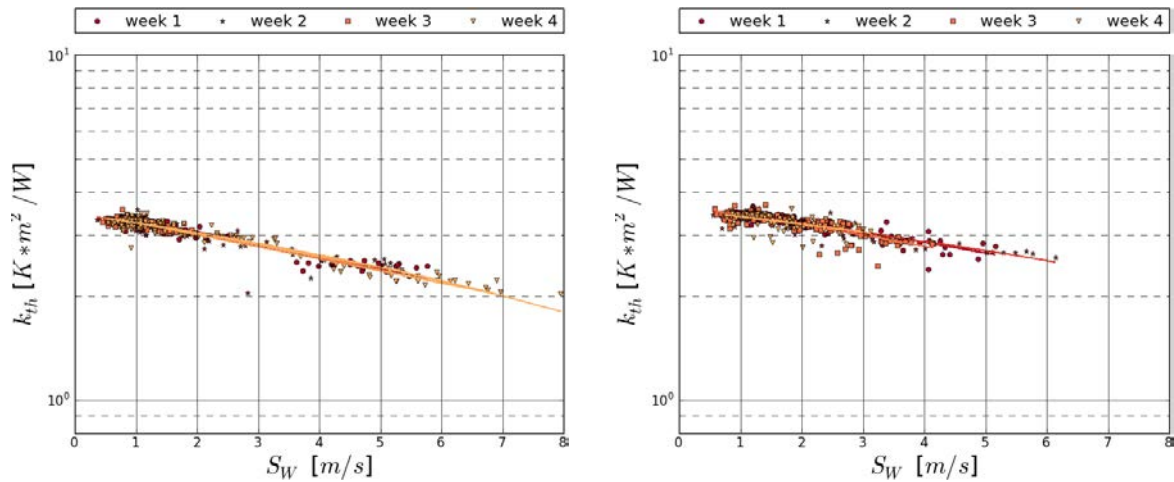
(a) Winter – 15/02-14/03/2012   (b) Late spring – 15/05-12/06/2012

Figure 17: Equivalent thermal resistance (k$_{th}$) versus wind speed (S$_W$) for 15 minute averages from IT1 (rack-mounted, freely ventilated, see Annex A); different subsequent weeks in February/March and May/June 2012

Figure 18a shows the temperature difference versus reference yield and Figure 18b the equivalent thermal resistance versus wind speed. The data originate from an installation in Ontario, Canada where high wind speeds regularly correlate with high reference yield as for the shown samples from week 4. Here again the equivalent thermal resistance is generally changing very little and it decreases exponentially with increasing wind speed (week 4).
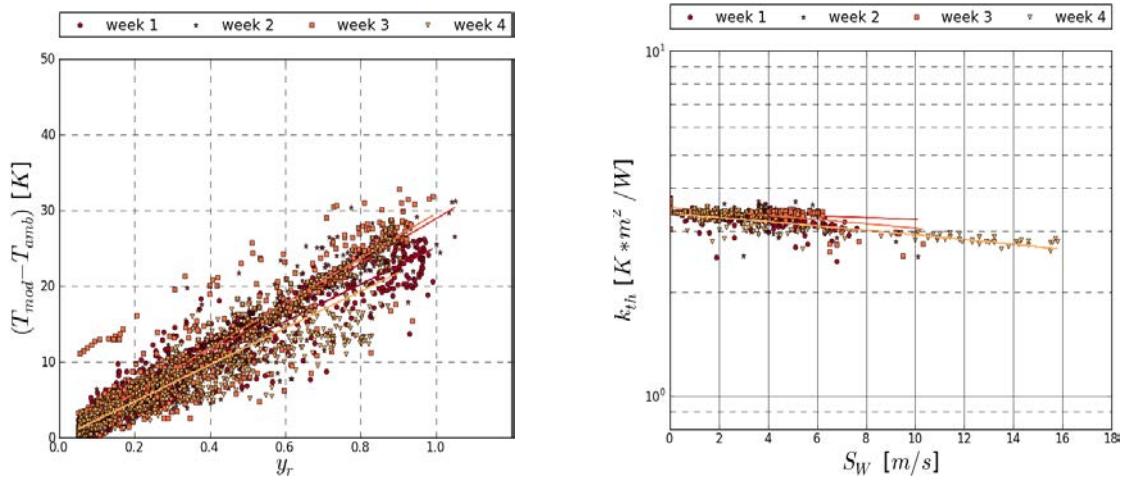
(a) Temperature difference   (b) Equivalent thermal resistance

Figure 18: Set of 5 minute average data characterizing the thermal behavior of CA1 (façade-integrated awning, see Annex A); different subsequent weeks in April 2011

Practical Use

As discussed above, the effect of wind speed on the PV system performance may be considered secondary. Moreover, often it is not measured on the site of a PV installation.

29

Nevertheless, if wind speed is available along with module and ambient temperature, the combination of these three allows fitting a simple though precise thermal model of the installation. The model can serve as a reference and for extrapolation with similar mounting arrangement. And it can serve for temperature normalization of performance date, for example when calculating expected yield during operations.

2.2.8 DC Voltage and Module Temperature

Analytical Description

The open circuit voltage (V_{OC}) of a solar cell and, hence, of a PV module, linearly depends on the module temperature (T_{mod}). The dependency on T_{mod} is stronger than any other dependency of V_{OC}, and hence, as a first approximation, it may be applied to the PV array output voltage V_{DC}. Under ideal operating conditions V_{DC} is equal to the MPP voltage of the PV array. Notably, this approximation is applicable only above significant irradiance levels. For very low irradiance, e.g., under twilight, V_{OC} and V_{DC} also decrease with decreasing irradiance.

Based on the linear relationship proposed above, the V_{DC} in an operational grid-connected PV system can be approximated as

$$V_{DC} = V_{STC} (1 + \beta \Delta T), \tag{7}$$

with
V_{DC} PV array output voltage (V_{MPP} under normal operating conditions),
V_{STC} PV array voltage at standard test conditions,
ΔT $T_{mod} - T_{STC}$ the module temperature above 25 °C standard test conditions,
β temperature coefficient of voltage (usually negative).

Plotting a scatter plot of V_{DC} versus T_{mod} together with a regression line for each week (Figure 19) allows identifying β as the slope of such a line. As long as the measured PV array output voltage is close to the MPP voltage the recorded samples should be situated on this line whose slope and intercept should stay approximately constant over time. Consequently, any sample away from this line points towards deviations from the common MPP.

Examples and Interpretation

The voltage-temperature correlation presented in Figure 19 was very high in the first three weeks of April. In week 4, many samples appear with very low array voltage while most samples still follow the linear relationship determined before. The phenomenon persisted throughout May.

A site visit has shown that this phenomenon was caused by a scaffold tower nearby, which had been put up in this week. The scaffold led to partial shading of the PV array and, as a consequence, the array was no longer operated at its MPP for homogeneous illumination. Since the shadow effects were relatively small, they could not be easily identified from the plots of system yield versus reference yield or performance ratio versus temperature. Only the deviation of array voltage clearly indicated the abnormal operation.

In normal operating conditions, this relationship is very pronounced for crystalline silicon (see Figure 20a) which is the reason why abnormal operation can be easily detected. Notably for other PV module technologies like CIGS (Figure 20b) the temperature-dependence of PV array output voltage is smaller. Moreover, in this example, the correlation in measurements is less pronounced, a hint that the voltage may be affected by other factors more than this is the case for crystalline silicon. Nevertheless, the correlation lines in Figure 20b are close to each other and irregular values of PV array output voltage as we see them for the installation in Figure 19 would become clearly visible for this installation as well.

(a) April 2010   (b) May 2010
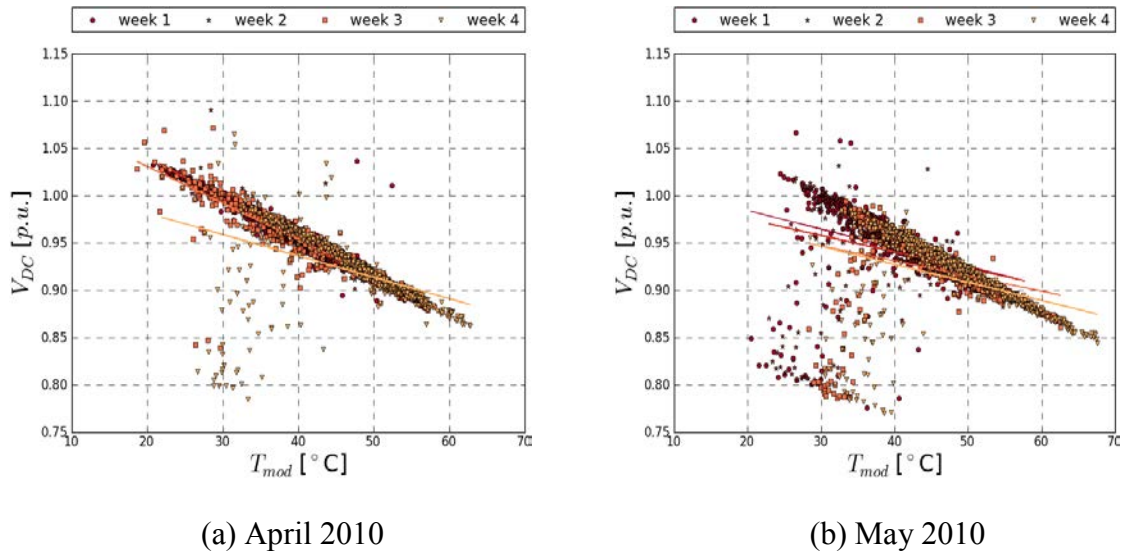
Figure 19: PV array output voltage normalized to MPP voltage versus module temperature for 5 minute averages from ES1 (see Annex A); different subsequent weeks April and May 2010

(a) Crystalline Silicon (IT1)   (b) CIGS (IT2)

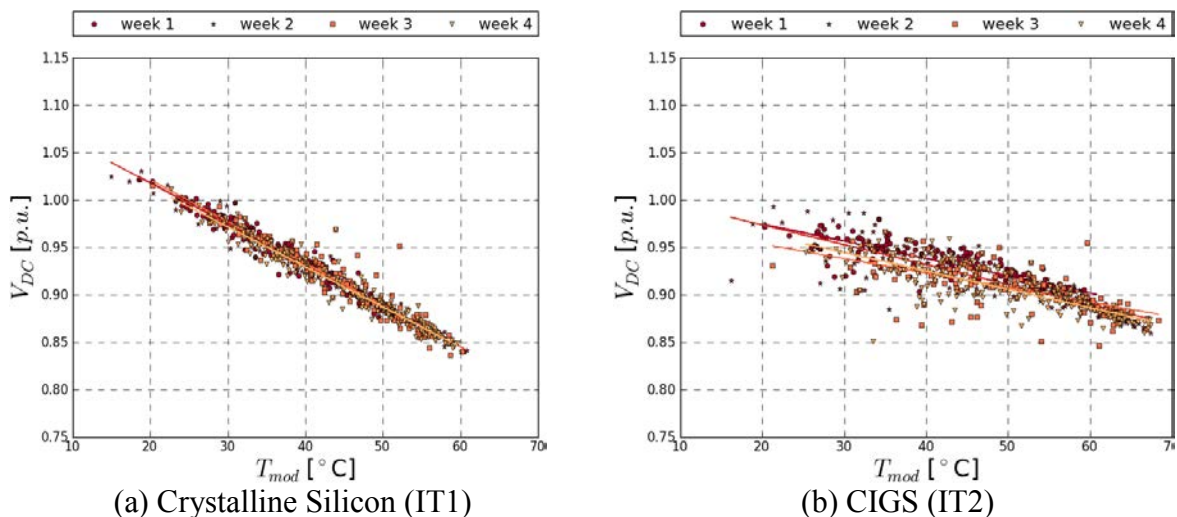Figure 20: PV array output voltage normalized to MPP voltage versus module temperature for 15 minute averages; comparison of crystalline silicon (IT1) and CIGS (IT2) (see Annex A); subsequent weeks from 15/04-13/05/2012

Practical Use

The array output voltage is more specific than the power values (y_f, y_A, y_r) that have been regarded up to know. As illustrated by the examples above, it

complements the data set by information on the operating points of the equipment. Notably this goes beyond MPP tracking. Phenomena that would manifest themselves are, e.g.:

- Situations where the inverter does not find the actual MPP.
- Situations with inhomogeneous illumination even if the actual MPP is found.
- Power limitation by the inverter.
- Short-circuited solar cells or bypass diodes.
- Any kind of inverter outage.

Therefore, in conclusion, PV array voltage is the most important electrical parameters to be monitored after the parameters required for final yield and reference yield.

2.2.9 Resilience of the Grid Voltage to Active Power

Analytical Description

In a grid-connected PV system, the utility grid voltage (V_{AC}) is usually considered an external quantity. It depends on the voltage set-point of the substation, the impedance of the feeder to which the PV installation is connected, and the power withdrawals and injections by other grid users connected to the feeder. Notably, its value over time is not entirely independent from the PV power to the utility grid (P_{AC}). A net power injection at a given connection point causes a voltage increase Δv_{AC} at this point, proportional to the power injected. For a PV system that is much smaller than the maximum overall demand on the feeder, this voltage increase is usually not easily visible. However, if the PV system is relatively large, or if many small systems in an area are connected to the same feeder, the relationship between voltage increase and PV power to the grid becomes visible.

The relative voltage increase as a function of system yield in an operational grid-connected PV system can be approximated as:

$$\Delta v_{AC} = \frac{V_{AC} - V_0}{V_0} = z \cdot y_f,$$

(8)

with
Δv_{AC} the voltage rise at the connection point (normalized),
V_{AC} the utility grid voltage at the connection point,
V_0 the nominal utility grid voltage,
y_f the system yield and
z the virtual grid impedance at the connection point (normalized).

Equation (8) characterizes the distribution feeder to which the PV installation is connected rather than the operation of the PV installation itself. If z is low, the grid voltage is resilient and the grid can absorb much PV power before the maximum voltage threshold may be approached. If z is high, the feeder has a high resistance or it already contains a high installed PV capacity whose simultaneous power injection has visible effect on the voltage. This is true for a given status of the grid and if no reactive power is provided at the injection point, i.e., the power factor is one.

As before, linear regression allows approximating the equivalent grid impedance *z* by the slope of the regression line. Figure 21 shows measured data of the grid voltage versus the system yield. The spreads of the different scatter clouds are relatively high, mainly because the grid voltage also depends on unknown external factors with statistically independent properties. Nevertheless, the slope and positive correlation between grid voltage and PV power to the grid is clearly visible for both cases. In Figure 21 many points with v_{AC} of up to 1.1 p.u. can be observed but no values above. Detailed observations have shown that the voltage threshold of 1.1 p.u. has been achieved several times and that the inverter then had tripped immediately. From data with longer recording periods, like with the hourly recordings shown below, these events can often not be reconstructed.

Regression of the equivalent grid impedance solves this problem as it allows extrapolating the grid voltage for higher system yield values than measured. Although the phases do not behave identically, in both phases the voltage threshold is approached for high system yield in weeks 1 and 4.

(a) Phase 1   (b) Phase 3
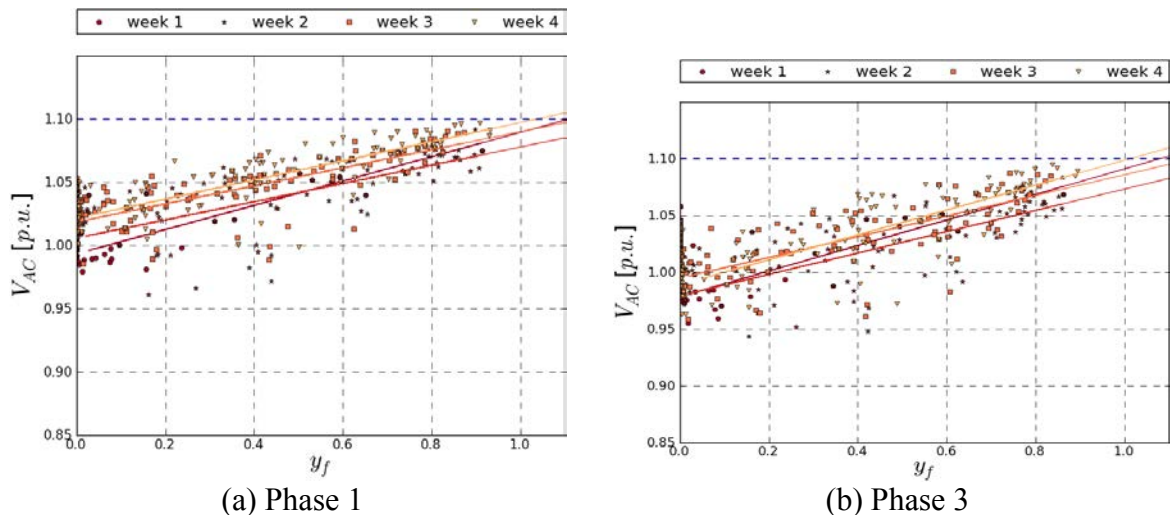
Figure 21: Utility grid voltage versus system yield for two inverters connected to different phases; hourly averages from FR1; different subsequent weeks in September 2010

(a) Sweden (SE2), May 2012	(b) Norway (NO2), July 2012
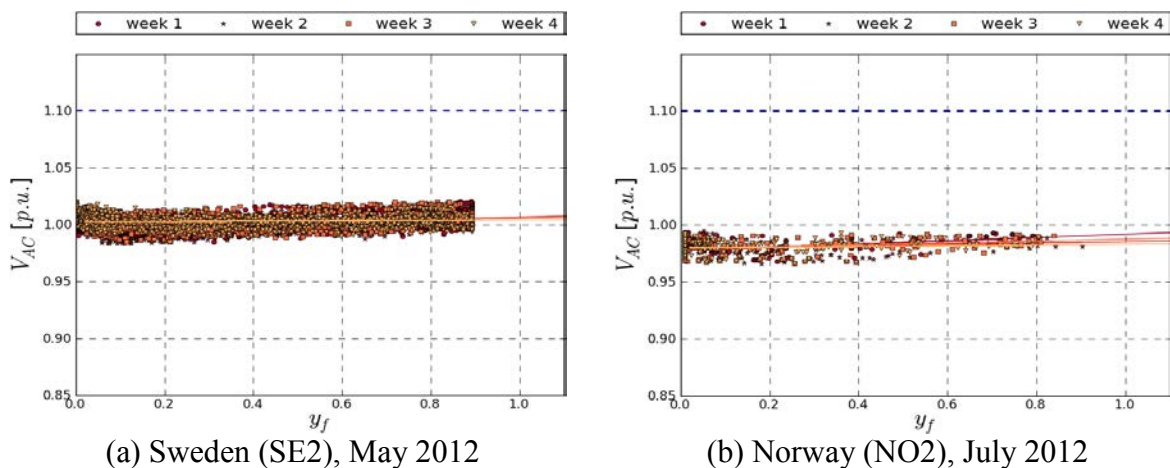
Figure 22: Utility grid voltage versus system yield for different systems;
(a) Stockholm, Sweden, 5-minute averages, and (b) Southern Norway, hourly
averages (see Annex A)

In all other data sets we have reviewed during this work, the slope is much lower than in the previous example, and the grid voltage never exceeds 1.05 p.u. For illustration, Figure 22 shows the same relationships for two other sites, both in Northern Europe. For the site in Sweden (Figure 22a) a slight but consistent slope can be observed over the weeks but the voltage threshold is never even approached. For the site in Norway, (Figure 22b) the slope is not significant. At this site, the grid is operated at a relatively low voltage of around 0.98 p.u., i.e., below the nominal value. Here, the voltage is virtually independent from the PV power to the utility grid.

Practical Use

As discussed along with the examples above, the relationship of utility grid voltage versus PV power to the grid illustrates the resilience of the grid voltage to active power. It is relevant when the capacity of the distribution grid for hosting PV is approached and the installations may trip from time to time. This relationship can serve to

- evaluate whether the voltage threshold is approached,
- extrapolate at which power injection to the utility grid the inverter is expected to trip,
- compare this phenomenon for different phases,
- estimate how much more PV could be connected at a point before the voltage thresholds would be reached regularly.

2.3 Conclusions for PV System Modeling

The views and models shown in the previous subsections allow for characterizing a PV system in physical terms and based on the observed operational behavior of the most important quantities measured. Based on simplified physical relationships linear model parameters can be derived from the measurements. The selection presented here covers the full energy conversion chain of a PV system. The analysis may serve for identifying and interpreting common design flaws and operational problems or simply for documenting the proper operation of the installation.

What is presented here based on simple mathematics for some exemplary installations may also be implemented systematically into software. It may be applied online for operational monitoring or offline for data analysis or for deriving PV component model parameters from measured data. Applied this way, periodic linear regression modeling is a powerful yet simple tool for interpreting your masses of data. Notably, in order to keep the complexity manageable for readers targeted with this report we intentionally did not introduce more sophisticated models as they are used for scientific evaluation or implemented in PV modeling software.

For visual analysis, much information can already be revealed when depicting scatter plots of two measured or derived parameters in two-dimensional Cartesian coordinates. Such a "stamp collection" can reveal interesting details for a given PV installation. It can serve as a visual tool to grasp operational characteristics of the system, indicating normal and abnormal modes of operation without immediately entering the field of physical PV system modeling. Depending on how well the monitoring system is equipped, deeper analysis can be performed leading to easier and timely identification of flaws and shorter reaction times.

Notably, this section elaborates on the stamp collection approach for plotting and periodic linear regression for mathematical assessment only, as these methods have actually been applied to the available data in the IEA PVPS Task 13. As discussed before, other approaches for data analysis are available as well as they have been introduced in Section 0. The Sophisticated Verification (SV) method allows identifying 12 kinds of system losses based on the fundamental system specifications and data for seven simple measurable quantities. The fault detection routine (FDR) can assess the likelihood of different failures along with the footprint method, that serves for analysis of patterns in dependency of power, time of the day and solar elevation.

3 Understanding Effects Related to Special Technologies

3.1 Comparison to Crystalline Technologies

This sub-activity was focused on the analysis of modules and systems based on materials other than crystalline silicon (c-Si). Points of interest are on one hand whether these technologies require other tools for a reliable performance prediction than c-Si devices and on the other hand whether they show specific aging properties diverging from those of c-Si.

Test Stands for Module and System Analysis

To establish an own data base for dedicated studies, data from a module test bench in Grimstad, from system test stands at Krustiansand/Norway and at the airport Bolzano-Dolomiti (ABD) are collected [49] [50]. Under test are, besides c-Si-modules, modules based on amorphous silicon (a-Si), CIS, CdTe and HIT material.

Figure 23: The system test facility at Bolzano (left) and the module test bench at Grimstad (right)

Table 5 and Table 6 give the data registered at the sites.

Table 5: Data registered at the Grimstad test bench.

Operation conditions	in-plane irradiance (Pyranometer), G	electrical parameters	short circuit current , I_sc
	ambient temperature ,T		open circuit voltage, V_oc
	back of module temperature, T_mod		voltage at MPP, V_mpp
			power at MPP, P_mpp

Table 6: Bolzano system test facility.

Operation conditions	global, dif. dir. hor. irradiance	electrical parameters	U_dc, I_dc, P_ac
	in plane irradiance		
	ambient temperature		
	back of module temperature		

3.2 Analysis of Seasonal Performance Variations

3.2.1 Application of a Standard Model for Performance Modeling

The data from the system at Grimstad had been used to evaluate whether the approach for the performance modeling established for c-Si technologies is applicable for the non-c-Si technologies. A respective modeling approach is given here by two modeling steps. First the short-circuit current is determined in dependence on global in-plane irradiance G and module temperature T_{mod} involving two parameters c_0 and c_1

$$I_{sc} = c_0 \cdot G \cdot (1 + c_1 (T_{mod} - 25°C)). \tag{9}$$

The power output of the module is then given by:

$$\frac{P_{MPP}}{I_{SC}} = (a_1 + a_2 \cdot I_{SC} + a_3 \ln(I_{SC} \cdot \frac{1}{A})) \cdot (1 + \alpha(T_{mod} - 25°C)) \tag{10}$$

which involves the 4 parameters a1, a2, a3 and α.

This approach proved sufficient for the modeling of a CIS Module. Figure 24 shows the relative bias of the modeled monthly energy gain when using a unique parameter set. Relative bias refers to the absolute bias of the computed monthly energy yield divided by the measured value. In this case the parameter set was fitted to the data from the month of July.

Figure 24: Monthly model quality (relative bias) for a CIS-module resulting from the application of a unique parameter set

This result proves that this performance model is applicable for CIS.

For an a-Si and a HIT module the model fails. This could be traced back to the insufficient representation of the short circuit current which fails to be properly described by a purely linear model in dependence on the global in-plane irradiance (see Figure 25).
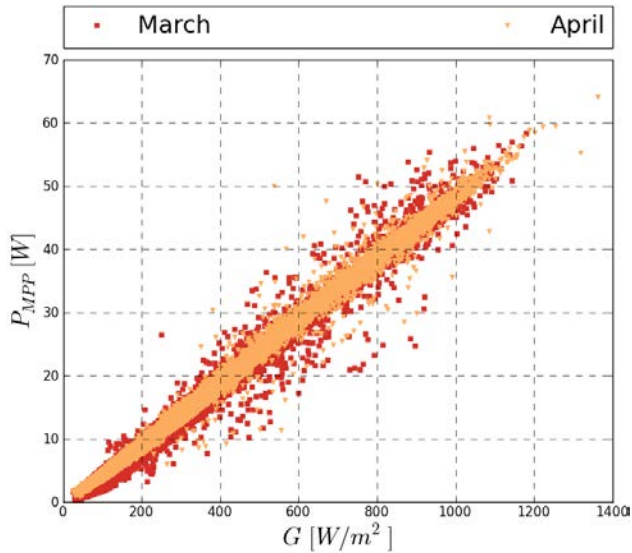
Figure 25: Power output of an a-Si module versus global in plane irradiance for two month of data

3.2.2 Model Extension for Modules using Amorphous Silicon

The increased variability of the short-circuit response is assigned to the spectral response of the material. A first approach to take this into account is to include the air-mass as a parameter influencing the spectrum as additional parameter in the modeling. Figure 26 shows the short circuit response I_{sc}/G for the a-Si module as function of air-mass.
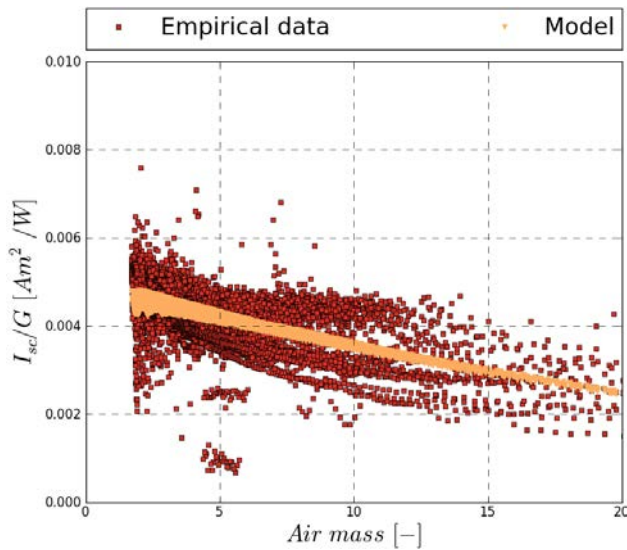
Figure 26: Short circuit response I_{sc}/G for the a-Si module as function of air-mass. Given are the empirical data and results from a respective model see below).

The variability of this response can be partly reflected by the following model:

$$I_{sc} = c_0 \cdot G \cdot \exp(c_1 \cdot AM) \cdot (1 + c_2(T_{mod} - 25°C)). \tag{11}$$

which takes the air-mass AM as an additional parameter.

The application of this model gives satisfactory results, given that the parameters are adapted to the data of the month under consideration. When applying this data set to other month the results show an increase of relative bias (see Figure 27).
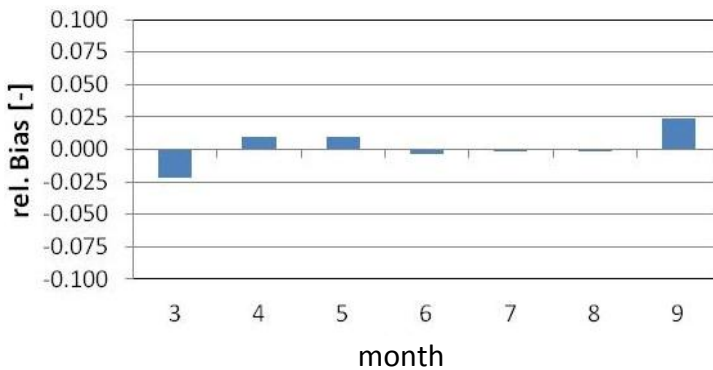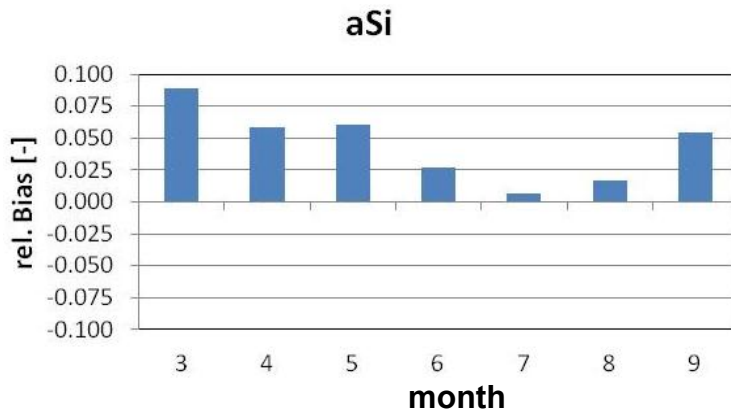

Figure 27: Monthly model quality (relative bias) for an a-Si-module resulting from the application of a unique parameter set, fitted here to the month of July

This calls for additional parameters to parameterize the short-circuit response. One option is to take into account the response to the direct and the diffuse irradiance separately. Figure 28 gives the power response of the a-Si system in Bolzano with respect to the diffuse fraction.
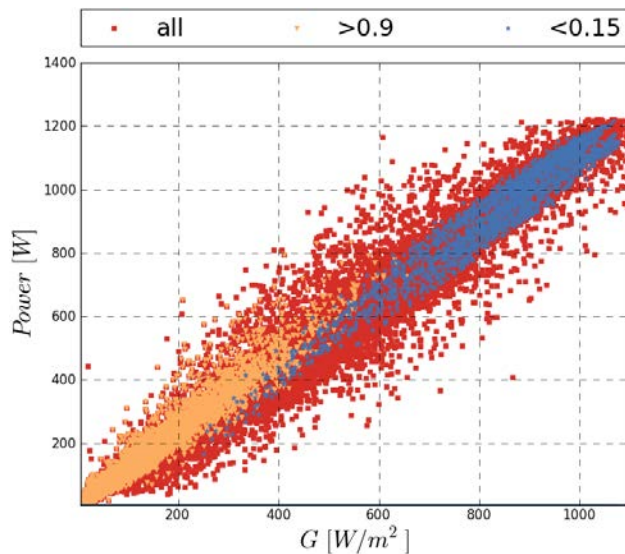
Figure 28: Power response of the a-Si system at Bolzano separated according to the diffuse fraction

A model reflecting this dependency was developed with the help of a data set kindly made available by the University of Oldenburg/Germany. This set comprises the short circuit current of an a-Si module mounted horizontally and the respective direct and diffuse irradiance. Based on this set the short circuit response can be modeled separately for the direct and diffuse component:

$$I_{sc} = G_{dir}\, c_0\, e^{c_1\, AM} \left(1 + c_2(T_{mod} - 25°C)\right) \left(1 - c_3(1/\cos\theta_z - 1)\right)$$
$$+ \quad G_{dif}\, d_0\, e^{d_1\, AM} \left(1 + c_2(T_{mod} - 25°C)\right) \left(1 + d_2 k_t\right)$$

(12)

with

G_{dir}	direct irradiance,
G_{dif}	diffuse irradiance,
T_{mod}	module temperature,
θ_z	solar zenith angle,
k_t	instantaneous clearness index and
$c_0, c_1, c_2, c_3, d_0, d_1, d_2$	empirical coefficients.

The application of this model looks promising. Figure 29 gives the measured and modeled short circuit response of the module in Oldenburg for the month of November. The model is applied with the parameter set fitted to the month of September and gives a good coverage of the variability of the response.
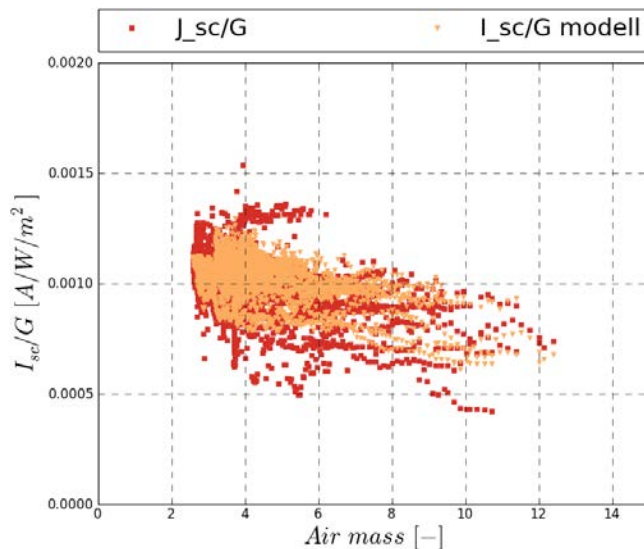
Figure 29: Measured (red) and modeled (orange) ratio of I_{sc}/G for an a-Si module as function of air-mass; data are for the month of November; model parameters are fitted to the set for November

This approach is used to model the power output of the system at Bolzano. Modifications had been necessary due to the fact that the modules of the generator in Bolzano are installed with a tilt and instead of the short circuit current, only the DC current of the system at maximum power point is available for the model definition. Figure 30 gives the modeling quality by the scatter plot of modeled versus measured power output for the month of August 2011. This work is currently ongoing.
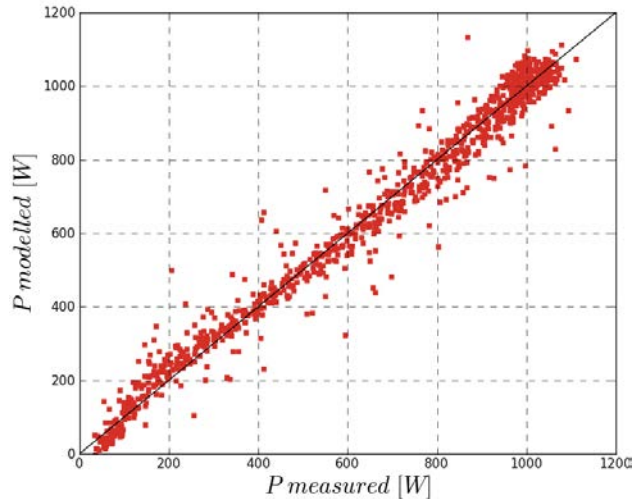
Figure 30: Scatter plot of modeled and measured power output of the a-Si system operated at Bolzano (month of August 2011)

3.2.3 Conclusion and Outlook on Seasonal Performance Modeling

Concerning the performance modeling over time scales of months, it could be shown that for CIS technologies no major modification is necessary. For modules involving a-Si material, major modifications are necessary to take into account the sensitivity to the spectral composition of the incoming light. Within the task, methods to take into account the spectral response in the absence of dedicated spectral measurements have been developed and tested. First results look promising, but further efforts are necessary for a well-founded confirmation.

For applying these models, a clear distinction between the performance variations due to meteorological causes and the ones due to changes or degradation in material is necessary. For further reading we refer to previous publications by the authors ([51]–[55]).

4 PV System Performance Improvement

4.1 Baseline Performance of Today's PV Systems

4.1.1 Performance Indicators and Typical Losses

The performance ratio is one of the most important variables for evaluating the overall behavior of a PV plant. The *PR* informs you as to how energy efficient and reliable your PV plant is. With the performance ratio one can compare the energy output of a PV plant with that of other PV plants or monitor the status of a PV plant over a prolonged period. It provides the operator with the option of checking performance, output, seasonal oscillations and long-term degradation.

Apart from the *PR*, other indicators for the operational performance of a PV plant have been proposed and are applied in practice. For example, AC efficiency has been proposed in [56]. AC efficiency is the overall energy conversion efficiency of the PV system. The AC efficiency depends on the array area instead of the module power rating, as it is the case for *PR*. This work exclusively uses *PR* as performance indicator but we encourage further studies on the advantages and disadvantages of this and other parameters for reporting on PV system performance.

Performance characteristics of PV modules used in the calculation (nominal power) of the performance ratio are determined under standard test conditions (1000 W/m² solar irradiance and 25°C module temperature, Air Mass 1.5 spectrum). Several variables can thus contribute to the final output from a plant and have an influence on the overall plant performance which may differ from what was estimated during the initial design. The performance of the power plant depends on several parameters including the site location, solar insolation levels, climatic conditions specially temperature, and several loss mechanisms (e.g. in cabling, module mismatch, soiling losses, MPPT losses, transformer losses and the inverter losses). There could also be losses due to grid unavailability and the module degradation through aging. Some of these are specified by the manufacturer, such as the dependence of power output on temperature, known as temperature coefficient.

More specifically, as seen in the case studies presented in Section 2, the following factors can influence the *PR* value:

- Temperature of the PV module and ventilation.
- Solar irradiation and power dissipation.
- Irradiance sensor or the PV module is in the shade or soiled.
- Recording period.
- Conduction losses.
- Efficiency of the PV modules.
- Efficiency of the inverter.
- Spectral mismatch between reference cell and the PV modules.
- Orientation of the solar irradiance sensor.

4.1.2 Typical Losses

The specific plant losses are described through capture losses (L_C) and system losses (L_S). Capture losses are caused, e.g., by attenuation of the incoming light (soiling, shading, reflection, etc), temperature dependence, electrical mismatching, parasitic resistances in photovoltaic modules and imperfect MPP tracking. System losses are caused, e.g., by wiring, inverter, transformer conversion losses, downtime. When designing and installing a PV system, it's important to make decisions that will maximize the energy that will be extracted from the PV array. This means accounting for, and minimizing, losses associated with a variety of system components. Typical loss factors are given in literature and used in software such as PVWATTS.

One of the first empirical analyses of losses in PV systems was published in [57]. A recent and detailed overview of loss factors typically occurring in practice has, e.g., been published in [58]. The loss factors in Table 7 were estimated from measured losses and component specifications. Thus, the table provides ranges for loss factors that might be encountered in practice.

Table 7: Loss factors observed in the field (see [58])

Cause	Typical	Low	High
PV module nameplate DC rating	0.95	0.88	0.96
Inverter and Transformer	0.92	0.88	0.96
Mismatch	0.98	0.97	0.99
Diodes and connections	0.995	0.99	0.997
DC Wiring	0.98	0.97	0.99
AC wiring	0.99	0.98	0.993
Soiling	0.95	0.30	0.995
System availability	0.98	0.00	0.995
Shading	0.95	0.00	1.00
Sun-Tracking	1	0.95	1.35
Age	1	0.70	1.00
Overall DC-to-AC Derating	0.77	0.00	0.88

The most important causes for reduced *PR* values are briefly explained in the following paragraphs.

Temperature: Module output power reduces as module temperature increases. When integrated into a roof, a PV module will heat up substantially, reaching back of the module temperatures of up to 80 ^{o}C depending on whether air gaps are present or not to exploit natural ventilation [59].

Dirt and dust: Dirt and dust can accumulate on the solar module surface, blocking some of the sunlight and reducing output. Although typical dirt and dust is cleaned off during every rain event, it is more realistic to estimate system output taking into account the reduction due to dust build-up during dry periods. Depending on the location, soiling can account for up to 70% of all losses (see Table 7).

Mismatch and wiring losses: The maximum power output of the total PV array is always less than the sum of the maximum output of the individual modules. This difference is a result of slight inconsistencies in performance from one module to the next and the module mismatch can bring to at least a 2% loss in system power. Power is also lost to resistance in the system wiring. These losses should be kept to a minimum but it is difficult to keep these losses below 3% for the system [60].

DC to AC conversion losses: Some of the DC power generated by the PV module is lost in the conversion process to AC current. Modern inverters commonly used in residential PV systems have peak efficiencies of up to 98% indicated by their manufacturers.

4.1.3 Trends in PV Systems Performance

A tendency of increasing annual *PR* values during the past years has been observed in several studies (Table 8). Typical ranges of *PR* rose from reportedly 0.50 to 0.75 in the late 1980s, and 0.70 to 0.80 in the 1990s, to more than 0.80 nowadays. These early PV systems often did not generate the expected energy yield. Dominating performance constraints were defects of the DC installations, poor reliability or bad MPP tracking of inverters, long repair times and shading problems [3], [57]. Several studies have investigated the performance of PV systems providing insight about the trend in increasing *PR* and decreasing spread between low and high range values. In studies performed under the IEA PVPS Task 2 [6], [5], PV systems in 11 countries were analyzed during eight years of installation. In a study performed in year 2000 [6], 170 grid-connected PV systems were analyzed, where the average annual yield (Y_f) was found to fluctuate only slightly from one year to another. However, there was considerable scattering around these average values for individual systems. In fact, the annual *PR* differed significantly from plant to plant ranging between 0.25 and 0.90 with an average value of 0.66. This spread was due to system and component failure, shading effects, MPPT mismatch, badly oriented PV arrays and high module temperatures. It was found that well-maintained PV systems operating well showed an average *PR* value of typically 0.72 at an availability of 98%.

Table 8: Average values and ranges of performance ratio for installations from different decades

Installed	Location	Range of PR	Average PR	Reference
2000s	Taiwan	<0.3 - >0.9	0.74	[63]
1980s	Worldwide	0.50 - 0.75	Individual estimates	
1990s	Worldwide	0.25 - 0.90	0.66	[6]
1990s	Worldwide	0.50 - 0.85	0.65 - 0.70	[5]
1990s	Germany	0.38 - 0.88	0.67	[3]
2000s	France	0.52 - 0.96	0.76	[61]
2000s	Belgium	0.52 - 0.93	0.78	[62]
2000s	Taiwan	<0.3 - >0.9	0.74	[63]
2000s	Germany	0.70 - 0.90	0.84	[33]

Furthermore, for PV systems installed before 1995, the average PR was 0.65, while for newer installations, installed after 1995, the average *PR* was of 0.70. The improvements of PV system performance were due to more realistic PV module ratings, higher component efficiencies (e.g. inverter) and increased reliability of PV systems. Furthermore, the *PR* values of newer installations were spread between 0.50 to 0.85 where this interval decreased further during 1998 and 2002 as a result of improved quality of the newer systems [5].

In 2004, from the performance analysis of 235 grid-connected PV systems in Germany [3], a clear tendency to improved performance was also found for new PV installations. At the same time, the broad spread of annual *PR*, decreased, indicating improved quality of PV system performance.

In [64], [61] and [62] reviews of residential PV systems in France and Belgium, were published analyzing the operational data of 10,650 PV systems. After a mean exposure time of two years, the mean value of *PR* was found to be 0.76 in France and 0.78 in Belgium.
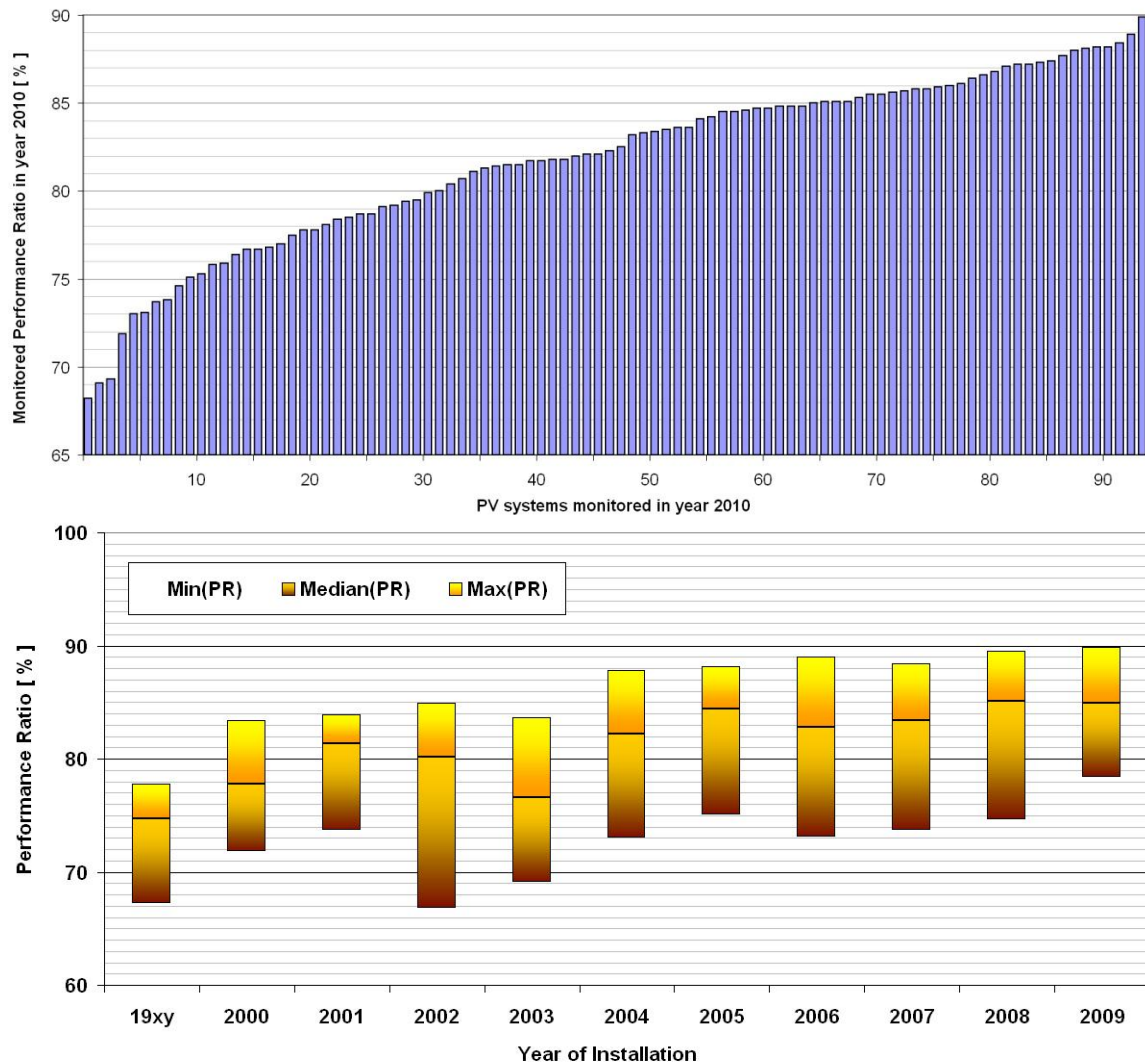
Figure 31: Historical development of PR over the past 10 years in Germany (from [33])

For another review of 2011 [63], three years of operational data of 202 grid-connected PV systems, such as monthly final energy yields and failure records, collected by ITRI in Taiwan were used to analyze the performance and system availability. The average *PR* value was 0.74, the average mean time to failure (*MTTF*) was found to be 3.96 years, average mean time to repair (*MTTR*) 65 days and the average availability 95.7%. The installation of real-time monitoring systems for PV plants was suggested to improve the system availability and *PR* value.

Finally, in a study performed in 2012 [33], *PR* of about 100 German PV system installations were investigated. Notably, a systematic influence on calculated *PR* values was found depending on the reference used to measure irradiance. Monitored *PR* is 2 to 4% systematically lower when calculated with irradiation data obtained by pyranometers compared to crystalline silicon cells. Annual *PR$_{Si}$* (subscript Si: measured with a crystalline silicon cell) for the approximately 100 systems for the year 2010 was found to be between 0.70 and 0.90 and showed a median *PR* of 0.84. For the case of German PV systems, "*good*" performances were above 0.84. An analysis of the historical development of *PRs* over the past

10 years (see Figure 31) revealed, however, that also in recent years (2007 and 2008) system designs were realized that showed PR_{Si} as low as 0.75, primarily dueto row shading and bad inverter performance. On the other hand, systems using highly efficient components and designed appropriately, as well as realized on the ground with good workmanship, showed PR_{Si} very close to 0.90. Loss heights of simulated loss mechanisms showed that even for highly performing systems, there is still room for some further optimization.

4.1.4 Long-term Reliability and Life Time Expectancy

In 2012, NREL reported long term reliability studies of photovoltaic modules which showed steadily improving degradation rates, with manufacturers offering over 25 years guarantee on their panels [65]. However, very few PV plants have been in existence for such a long period of time, for verification of the guarantee. Some reports have been published on this subject by NREL, Fraunhofer ISE and others. It is important for the PV industry to know the long term reliability, since it impacts the life of the PV system, and hence changes the cost considerations. NREL tests have concluded that the degradation and the losses in maximum power are almost entirely due to losses in short circuit current, and that these losses are almost identical for single and poly crystalline panels and are highly dependent on the process used in manufacturing. The drop in short circuit current by the modules can be attributed in part to the visually observable physical defects including EVA browning, delamination at the Si-cell/EVA interface and the occurrence of localized hot spots.

The most recent distribution for long term stability of performance (NREL study) has a mean value of 0.8%/year and a median of 0.5%/year where a decrease in performance is defined as a positive degradation rate. The majority of these reported rates, 78% of all data, are below a rate of 1%/year.

The data from long term tests showed that module degradation for 10 years can be in the range of 4 to 7%, lower than the 10% degradation currently guaranteed by most manufacturers. This information is extremely relevant during power plant design for getting an accurate estimate of the amount of power and therefore revenue to be expected each year after installation. The NREL study suggests that a more reasonable rule of thumb of degradation is less than 0.5% per year [65].

The methodology guidelines on life cycle assessment published by the IEA PVPS Task 12 recommend life expectancy used in life cycle assessment studies of photovoltaic components and systems as follows [66]:

- Modules: 30 years for mature module technologies (e.g. glass-tedlar encapsulation), life expectancy may be lower for foil-only encapsulation;
- Inverters: 15 years for small size plants (residential PV); 30 years with 10% of part replacement every 10 years (parts need to be specified) for large size plants (utility PV), (Mason et al. 2006);
- Structure: 30 years for roof-top and façades and between 30 to 60 years for ground mounted installations on metal supports. Sensitivity analyses should be carried out by varying the service life of ground mount supporting structures within the time span indicated;
- Cabling: 30 years.

One can conclude from all available data that the manufacturers provide a guarantee with a definite margin of safety and for design purposes a lower degradation percentage can be employed. Further, the length of warranty has continuously increased thus far, indicating the increase in confidence among manufacturers, as they manufacture products with durable quality, due to technology improvements and quality assurance practices. However, it should be noted that in the light of the very high cost pressure on PV installations, quality assurance measures including monitoring and (long term) performance analysis remain highly relevant, irrespective of these positive changes to the general outset.

It has been observed that the confidence among manufacturers has increased over time, with some of them giving a guarantee of only 10% degradation over a period of 12 years and 15% over 25 years. This is evident from the increase in guarantee period being provided by module manufacturers, as shown in the list below given by Wohlgemuth et al [67]:

- **Before 1987:** 5 years.
- **1987 to 1993:** 10 years.
- **1993 to 1999:** 20 years.
- **Since 1999:** 25 years.
- **Expected by 2015:** 30 years.

This has important consequences in calculation of electricity cost from the power plant. With increased lifetimes, one can expect better returns on investment. The quality of module is thus of immense importance.

4.2 Simulation to Ascertain Good System Design

PV system performance depends both on the components' properties and on design decisions. In contrast to component selections, benefits or disadvantages of design decisions must be determined by simulation in advance, typically based on time-step simulations of system behavior. Simulation approaches are well known and generally proven [32], [68], [69]. Typically they include the following components' properties: STC power (and bin width), module dependencies on irradiance level, temperature, angle of incidence and spectrum as well as several cable and inverter specifications.

Simulations can differentiate loss mechanisms that cannot be directly measured. A comparison of loss mechanisms resulting from such simulations and monitored performance data in the year 2010 is given for 10 exemplary systems all located in Germany in Figure 32 [33]. The data shown in Figure 32 lists loss mechanisms instead of PR values, so "$1 - PR$". Note that it is possible for some systems to calculate a PR for the AC-side (PR_{AC}) and the DC-side (PR_{DC}) separately, as in those systems monitoring equipment on the DC-side was installed (see two colors in bars representing monitored data).

Details of the simulation models usually vary. In the example given in Figure 34, the software Zenit of Fraunhofer ISE was used and the following assumptions made: For transformer losses (if present) and module-mismatch single loss factors of 1% and 0.8%, respectively, were assumed and for cabling losses the standard

assumption of fixed loss values of 1.5% for DC-wiring and 1% for AC wiring at maximum rated power. Spectral and reflection effects affect both the reference cell and the PV system and therefore are not relevant for the simulation itself. However, they are evaluated through a correction routine of the reference cell measurements to estimate PR_{Pyr}. Further details are given elsewhere [33].

Soiling effects are not considered, which can be (partly) reasoned by the assumption that frequent rainfall is likely to effectively clean modules.
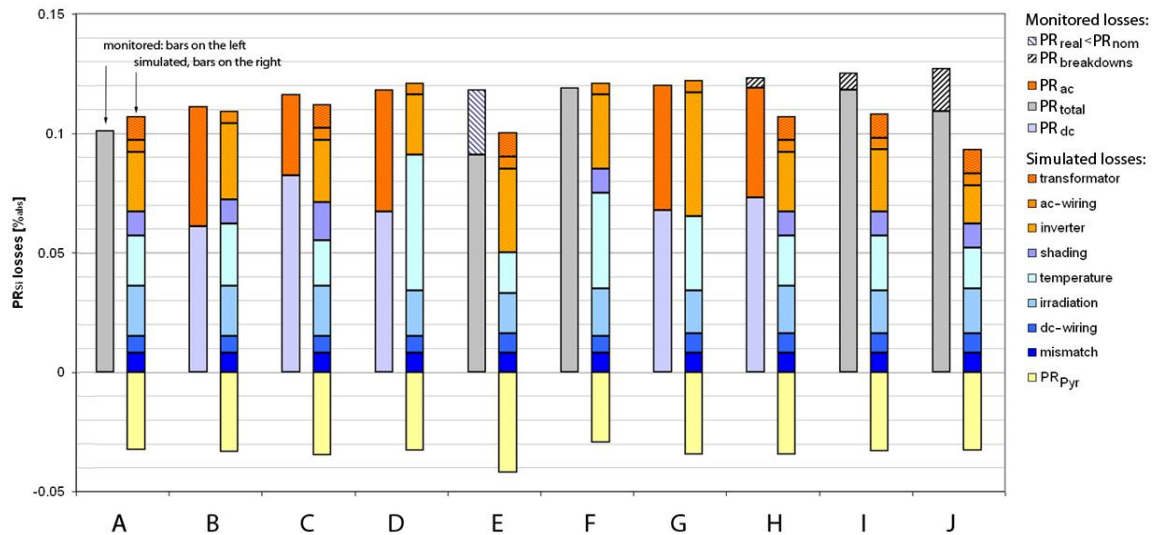
Figure 32: Detailed gains & losses for 10 systems resulting from system simulation and monitored yields. Details are given in the text.

The design decisions for large-scale systems mainly concern mounting angle and row distance (related to irradiance gains and shading losses), the inverter to module power ratio and cabling optimizations. These design options affect the overall system efficiency, commonly expressed as *PR*, as detailed in various previous sections.

The following two sub-sections highlight simulation examples on both shading losses (sub-section 5.2.1) and the inverter to module power ratio (sub-section 5.2.2). Finally, it is summarized how a full year's performance of a given component may be predicted from components' properties and meteorological conditions at a system's site: For PV modules, this approach is known as Energy Rating (ER), and here an overview of remaining uncertainties and the slightly reduced uncertainties of yield predictions when ER data is available are given.

4.2.1 Simulating Shading Losses

While optical shading could be estimated from multiple irradiance measurements, the electrical losses would require the measurement of individual IV curves for single modules or cell strings. For commercial PV systems, such measurements will not be available. Although there is no simple way to directly measure shading losses of a PV system, the shading losses may still be estimated using the so-called profile angle and simulations. The so-called profile angle is defined as the projection of the sun elevation onto a plane orthogonal to the azimuth orientation of the modules, see Figure 35.
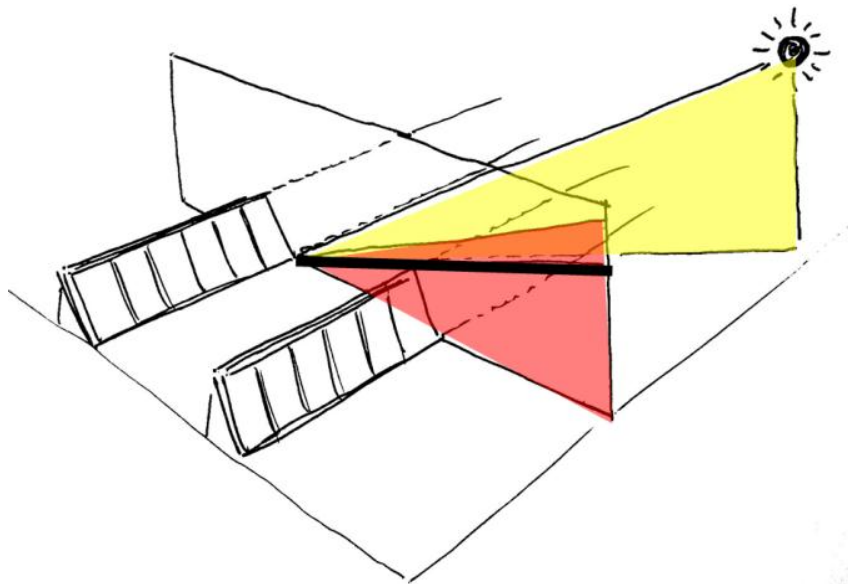
Figure 33: The profile angle is the projection of the solar elevation angle (yellow) onto a vertical plane orthogonal to the azimuth of the module rows (red); the thick black line denotes the minimum profile angle without shading ("shading angle")

To allow for a quantification of shading losses, a number of different average PR values are calculated: for when the profile angle is greater than the shading angle ($PR_{unshaded}$), for when the PR is smaller due to shading (PR_{shaded}), allowing to calculate the difference of these two PR values (PR_{drop}). The calculated quantity PR_{drop} still includes other loss effects in addition to shading, such as low light behavior of the modules and part load efficiency of the inverter. However, it can nonetheless be used as an estimator to compare different systems and locations, and it allows for an assessment of simulation accuracy for this specific loss mechanism. As irradiance data in the simulation measured irradiance in module plane ($G_{modmeas}$) and measured module temperature ($T_{modmeas}$) are used.

Shading losses are calculated as follows. Horizontal brightening modeled by the Perez model [70] is assumed to be fully lost, as this part of the sky is not visible from a second module row. Losses of the isotropic diffuse fraction are assumed to be the same for the whole module row. They are calculated according to the fraction of the field of view of a module row that is not "visible" due to the module row in front of the actual row.

To represent the electrical behavior of the PV modules, a simplified model is used to calculate the losses for the direct and the circumsolar components of solar irradiance. The module row is split up into electrically independent DC sections by taking the connection of module to module strings into account. So for instance a row of five modules on top of each other, connected to module strings horizontally will be represented by five independent sections, while in the case of a vertical connection to module strings, it would be represented by a single section only. Furthermore a "critical fraction" for every independent section of the row can be defined [71] dependent on the orientation of the modules. Within this critical fraction the shadow loss is assumed to increase linearly. When the critical fraction is reached, the section is assumed as fully shaded, i.e. there is only some remaining diffuse irradiance. Details on how to calculate the specific "critical fraction" are given elsewhere [71].

Now for every time step in the simulation it is checked for every independent section, whether the section is affected by shading and if so how much of the section is affected. If the section is shaded within the critical fraction, direct and circumsolar irradiance is reduced linearly, while it is assumed to be zero, if more than the critical fraction is affected by shading. The advantage of this approach is that it is applicable for different kinds of module technologies including thin film and that it needs not much computation time. However a more sophisticated approach as described in [72] can consider effects like shifts in the IV curves at various shading conditions and is better suitable to predict the MPP tracking of the inverter in such conditions.

As data for the analysis the full year 2011 was used. All times steps (measurement intervals) with a solar elevation less than 3° or a measured AC power below 10 W/kWp were removed. Also, a few days with (partial) system downtimes were removed. We selected three systems with different locations and configurations for our analysis. Table 9 shows the details.

Table 9: Systems considered for the shading analysis

	Latitude	Azimuth (south=180)	Slope	shading angle	Module assembly	Strings per MPPT
Syst. 1	48°	237°	27°	19°	portrait	1
Syst. 2	52°	170°	15°	9.5°	land-scape	3

Finally, the influence of the variation of the tilt angle and the orientation of the modules was analyzed, preserving row distances and installed power. This can be thought of as a simple optimization of a system of fixed power on a given fixed roof area, that will have almost no influences on costs or investments. For the optimization we started from the satellite data and calculated the system behavior for different tilt angles and for the alternative of PV modules mounted in landscape mode as illustrated in Figure 34. Figure 35 shows the results of this optimization for System 1. It turned out that the specific yield of this PV system could be increased by about 4% by moving the modules to landscape mode and reducing the tilt angle to 16°. The results for System 2 are shown in Figure 36. For System 2, at the given row distances, it would be more appropriate to increase the tilt angle of the modules to about 28° which would result in an about 3.5% higher yield.
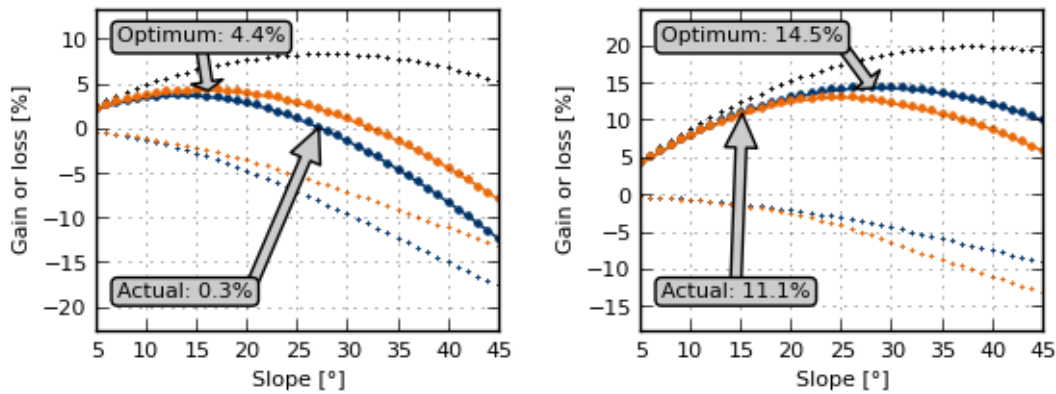
Figure 34: Optimization for the two systems: Values for the original system design are given in blue, while the values for the variation with modules mounted in portrait mode are shown in orange. The tilt gains are shown as black points again.
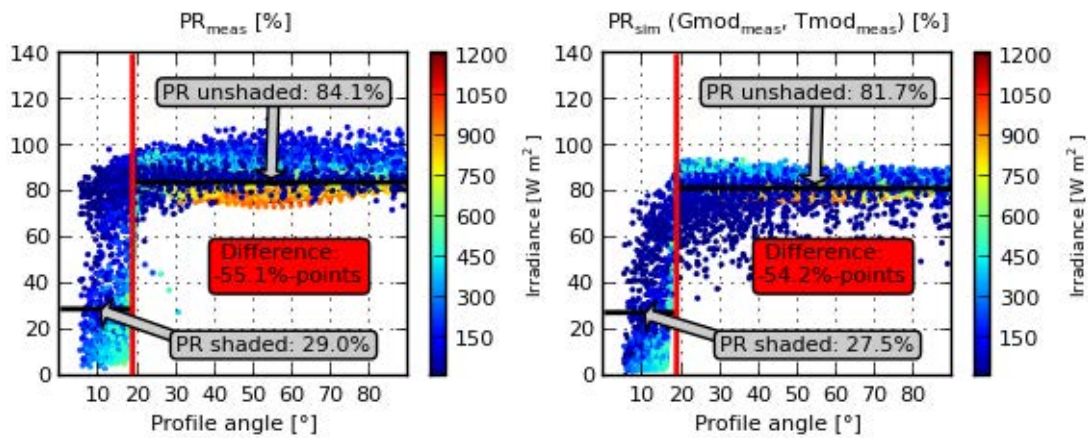
Figure 35: *PR* values and row shading losses of System 1, as measured (left) and as simulated from measured irradiance and module temperature (right).
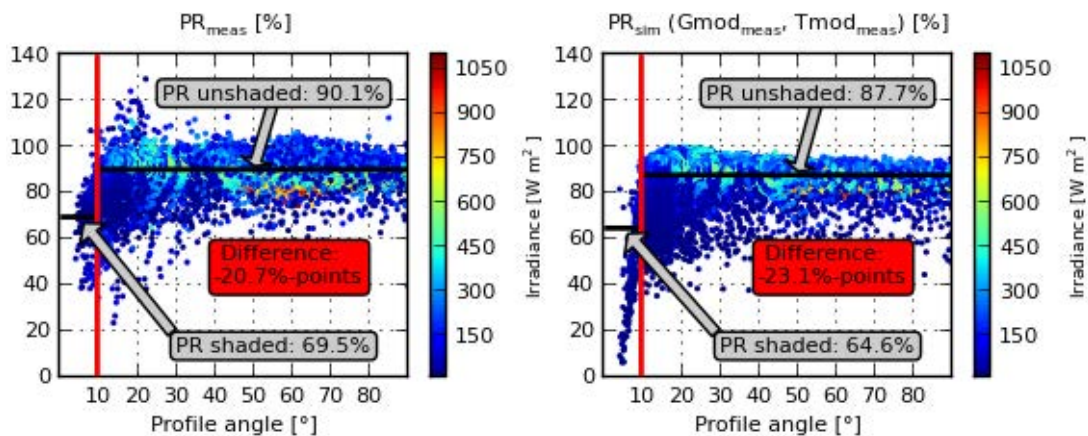
Figure 36: *PR* values and row shading losses of System 2, as measured (left) and as simulated from measured irradiance and module temperature (right).

4.2.2 Simulating Inverter Power Limitation Losses

Today's PV systems typically show an inverter being underrated with respect to the installed module power. This design option is chosen intentionally, as (under European conditions) a PV generator rarely operates at its nominal power. However, under some cold and sunny conditions, the inverter might limit the system output power.

This loss effect cannot be measured directly, but the amount of loss may be deduced indirectly. Figure 37 (left) shows full year performance data (blue dots for all 5-min intervals) of a PV system. Inverter power limitation is visible above 897 W/kWp. By using a method of *PR* extrapolation, we may deduce the energy loss caused by this limitation from measured values only. A first *PR* value is calculated for an irradiance range from 200 to 900 W/m² as 89.5%. A second *PR* value is calculated for the irradiance range from 900 to 1200 W/m² affected by inverter limitation, leading to 88.4%. Taking the difference of both values, weighted with the irradiation sum of each of the two ranges, the difference in *PR* is worth some 0.05% of annual energy output.

We also performed a simulation of PV system behavior for this system and varied the inverter power limit. Figure 37 (right) gives the results. For the actual PV to inverter ratio of 1.12, our model predicts limitation losses of 0.03%. Looking at the complete curve of losses between PV to inverter ratios of 0.9 and 1.3, a proper design may be confirmed for this system aspect. The inverter is just large enough to prevent this system design from significant power losses. In conclusion, the example system of Figure 37 is properly designed, as limitation losses are kept rather small.

Figure 37: On the left, specific AC output of a PV power plant vs. in-plane irradiance is shown, with blue dots denoting measured 5-min average values, orange showing simulation results and simulated AC power without inverter power limitation in red. On the right, power loss due to inverter power limitation vs. PV to inverter power ratio is shown for the same system.

4.2.3 Uncertainties of Energy Yield Predictions

Several modeling steps add to the total uncertainty of a PV system's yield estimation. These steps and their related uncertainties may be grouped into five categories:

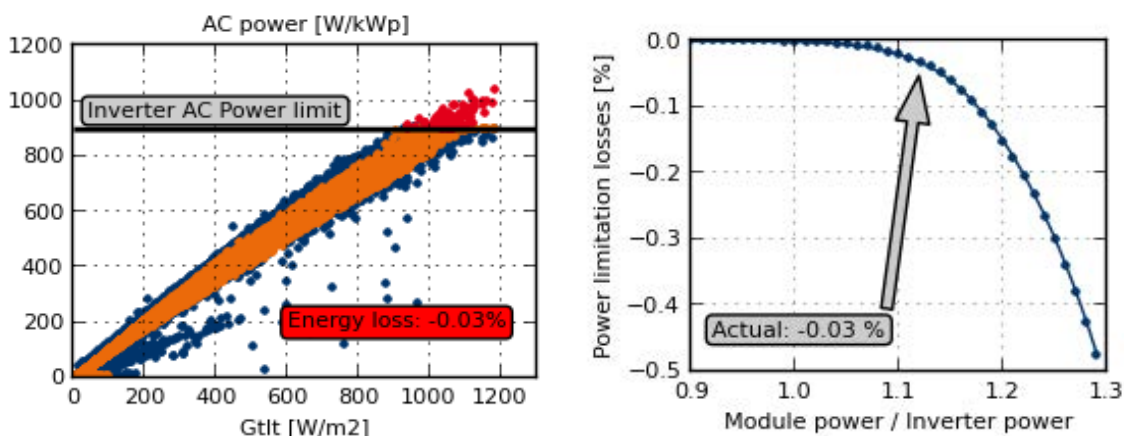- Energy Rating comprises the prediction of module behavior dependent on STC power, low light response, angular effects and spectral response under given meteorological conditions. The accuracy of ER calculations depends on the suitability of the numerical models as well as on the uncertainty of input component parameters. Typical uncertainties range from 0.5% to 2.5% [30].
- Performance Ratio prediction adds the influence of system design and BOS components to the ER results. So, besides shading losses, also inverter efficiencies and limitations and cable and transformer losses need to be considered. Again, typical uncertainties may range from 0.5% to 2.5% [30].
- Deviations from specifications (mainly with module STC power and low light response) also affect the uncertainty of actual system *PR*. STC power deviations may reach up to a few percent and are assumed to be nearly constant over all irradiance conditions.
- Module and system degradation affects the long term actual *PR*, as outlined in section 6.1.4. As degradation rates considerably vary from system to system [65], [73], there are relatively high uncertainties for single systems. Furthermore the influence of the degradation rate on the simulated *PR* is increasing with the lifetime of the system.
- Finally, the solar resource determines the long term actual yield of a PV system, and the uncertainties of solar resource figures add directly to the uncertainty of predicted energy output.

While typical yield estimations mention some 5% as overall uncertainty, this value might even be greater than 10% under certain conditions. However, in this contribution, we concentrate on design decisions; so, mainly uncertainties in *PR* prediction are of concern. When comparing prediction results to observed yields, there are additional measurement uncertainties. Pyranometer measurements are expected to be in an uncertainty range of ±2% [74], [75], while energy meters show uncertainties of ±0.1% to ±0.5%, see section 3.2.

As shown in [32], observed *PR* values agree with predicted values within a band of 2% to 3%. However this overall uncertainty in *PR* verification should not influence the simulation results strongly for single simulation steps.

4.2.4 Energy Rating and Reduced Uncertainties

At a first glance, the idea of Energy Rating (ER) seems compelling, as especially the ER label on the back of the module seems to make a statement to the actual energy output rather than the bare STC performance. Here, we will quantify the benefit of the ER label in terms of reduced uncertainties in energy yield predictions, when ER procedures have been applied to the modules.
The IEC 61853 standard describes the laboratory measurements that lead to achieving the "energy rating" of the modules. Theoretically, measurement results from the laboratory can be directly implemented in time-step based yield simulations. For this purpose, only the model describing the module efficiency as a function of light intensity needs to be adjusted to measured efficiencies over

irradiance intensities. Even a simplified calculation, without a time step simulation, is feasible: Divided sums of solar radiation bins can be multiplied with measured efficiency of the respective light intensity bin, analogue to Figure 38. This figure illustrates the energy annual distribution of solar radiation for locations in Northern and Southern Germany as well as Spain in 100 W/m^2 irradiance bins (the energies of the respective bins were summed up and normalized to 100% each, as naturally solar energy in Spain will be much larger as compared with e.g. Northern Germany).
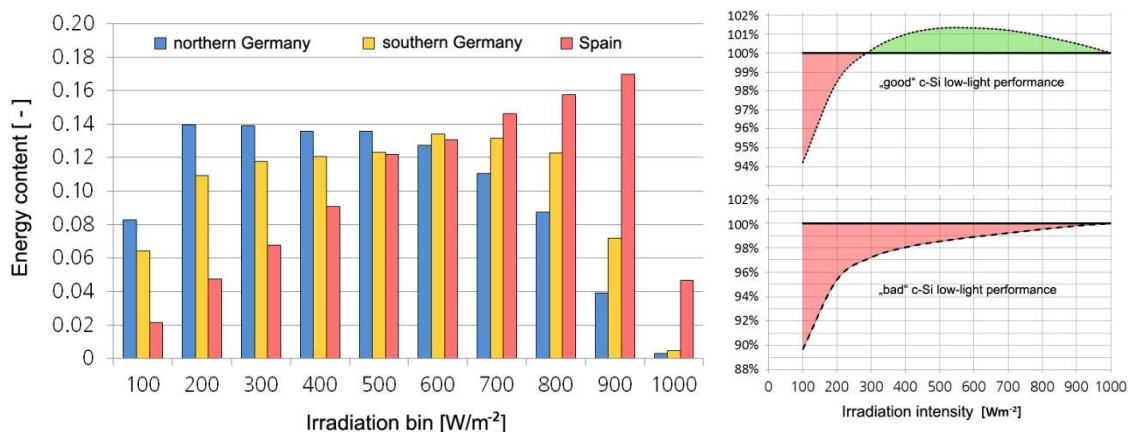
Figure 38: Distribution of solar energy as a function of irradiance intensity (left panel) for three locations and irradiance intensity dependent module efficiency (right panel) for two different modules of the same technology, reflecting both "good" and "bad" performance under low-light.

The distributions of solar energy as a function of irradiance intensity illustrate that for Northern Germany rather weak light intensities prevail; good module efficiency at low light intensities is therefore much more relevant for Northern Germany as it would be for sunny Spain. To calculate how much or little this low-light efficiency effect is in concrete terms on annual energy yield, two typical c-Si modules with divergent low-light performance are assumed, see right panel of Figure 38. The multiplication of the efficiency shown on the right panel with the light intensity distributions shown on the left panel (normalized to STC = 1000 W/m^2) result in the losses or gains listed in Table 10.

Table 11 summarizes all quantities and related uncertainties with and without the so-called module Energy Rating (ER). Clearly, the majority of listed values and which should be stated in energy yield assessments is not affected by the ER of the module.

In conclusion, the actual energy output of a module depends on a variety of factors, not directly connected to the modules' performance. The benefit of module ER is therefore only very limited. The reduction of uncertainty is estimated at around 0.5%, with typical uncertainties of figures stated in yield reports in total of about 5%.

The potential for enabling a further development of quality assurance measures is perhaps the greater benefit that an energy rating label brings with itself – should the indication of the ER be someday established as a standard indeed. So far, verifying shipped module performances by laboratory measurements is fairly cumbersome and hardly performed for more than randomly selected module

batches. This is particularly true when considering the fact that quite often different batches of cells can be laminated into modules of the same type. So far, only the power specifications at 800 W/m^2 (NOCT) and sometimes 200 W/m^2 are available. Here, using statistically selected samples, the ER label might allow for better power and especially performance verification measures, however, only related to the modules and not considering any system aspect.

Table 10: Simulated energy gains and energy losses related to different irradiance intensity distributions in combination with differing low-light performance of modules.

% Gain or loss	Northern Germany	Southern Germany	Spain
Low-light performance "good"	+0.0 ± 0.9	+0.2 ± 0.8	+0.6 ± 0.7
Low-light performance "bad"	–2.6 ± 0.9	–2.2 ± 0.8	–1.4 ± 0.7

Table 11: Reduction of uncertainties of individual loss mechanisms through the use of energy-rating measurements. The bandwidths of the individual uncertainties arise from plant-specific and site-dependent effects.

Loss mechanism	Uncertainty [%]	
	Without ER	With ER
Irradiation (horizontal)	3–5	equal
Direct/diffuse-ratio of irradiation	2–3	equal
Shading (incl. inverter behavior)	1–4	equal
Soiling	1–3	equal
Reflection	0–2	not yet investigated
Spectrum	0–2	not yet investigated
Low-light behavior	1–2	0.6–1.0
Temperature dependence	0–2	0.0–0.5
Module mismatch	0–1	equal
Cabling (DC and AC)	0–1	equal
Inverter	0–2	equal
Transformer	0–1	equal

4.3　Particularities for Special Technologies

Besides the necessary adoption of the schemes for the performance modeling for some thin-film technologies as described above, the treatment of non c-Si modules requires additional attention concerning the rating and characterization of stability/degradation. These needs had been identified in previous research collaborations e.g. the EU PERFORMANCE project see e.g. [40] and guidelines/rules entered into the standardization process. In the context of the

characterization of the PV system performance, these additional requirements identified for the module rating should get special attention.

Indoor characterization of thin-film modules requires – besides that special attention had to be paid to the conformity of the spectrum of the solar simulator – procedures for preconditioning as, e.g., described in IEC 61646, which sets rules for pre-test light soaking (see e.g. discussion in [76], [77], [78] and [79]). Other means to avoid the influence of meta-stability effect had been established at NREL ([80], [81]). These topics are in discussion in the renewal process by the standards commission. This development is followed by Task 13, ready to include repercussions of further developments to suggestions for best practice in module performance characterization.

4.4 Recommendations for Improved Performance

The performance of a PV system is clearly related to not one single but a variety of factors. Some of these factors are controllable, but some are not in the realm of human control. These can be further divided into the design and construction phase and the Operating and Maintenance (O&M) phase. With technical questions of yield simulations concerning the design phase already described in the previous sub-section 6.2, in this sub-section we discuss primarily the O&M phase of assuring improved PV performance.

It is worthwhile to note that achieving optimal performance is next to impossible without monitoring of the efficiency or Performance Ratio (*PR*, see previous sections) of the system. Only when monitoring exists, it is possible to ascertain that all systems are working as expected. When the *PR* drops, the operator must search for the reason for the drop, as to allow for improved performance. To this end, we will focus in particular on real-time monitoring as a means for improving performance. However, note that performance improvement can also be argued to be related to improved system design (see sub-section 6.2).

When looking at potential improvements, it can be helpful to differentiate factors that can actually be controlled from those that are simply beyond any control. These not entirely controllable factors inject a level of inaccuracy into any performance forecast and include:

- Solar irradiation.
- Ambient temperature.
- Wind speed and direction.
- The behavior of wildlife in the area.
- Vandalism.

Controllable factors are many in number, a partial list of those most important to performance include the following:

- Soiling accumulation – alleviated by washing panels.
- Quality of galvanic connections (DC and AC cabling) – alleviated by ensuring tight connections.
- Shading due to vegetation – alleviated by effective gardening.

- Inverter environment – shading of inverters in direct sunlight, dust accumulation on filters etc.
- Timely replacement of surge arrestors – ensuring that old or ruptured arrestors are replaced before they are required.
- Appropriate measures for keeping monitoring sensors in optimal conditions, see chapter 3.
- Inverter downtime – though the timing and frequency are not controllable, the recovery is controllable by efficient maintenance practices.

Improving performance requires efficiently managing those controllable factors in order to mitigate the negative aspects of the uncontrollable variables.

4.4.1 Real-time Monitoring

The first step is to ascertain the acceptable value for the efficiency or the *PR*. This acceptable value is calculated by the PV system designer, using commercially available specialized simulation tools that calculate the efficiency over the first year of operation taking into account all calculable losses, and most importantly, the losses due to module temperature. This value is often in the 80% range. It is good practice to calculate the *PR* for each different array configuration in a PV site. In the day-to-day operation of real time monitoring, these acceptable values can then be tested for.

To manage the efficiency of a PV system, it is imperative that the *PR* be calculated online in order to become aware of low efficiency as soon as possible. To this end, every system must be capable of monitoring the amount of solar irradiation that is incident onto the PV array and the module operating temperatures, as already extensively addressed in Section 3.

The *PR* includes losses due to heat. However, since we do not control the module temperature, this value does not represent the controllable quality of the system accurately. The module temperature is to be removed from the equation by multiplying the *PR* by the percentage of temperature correction.

A suggested method for calculating this temperature offset is to average the back panel temperature over 15 minutes, subtract this value by the STC temperature of 25°C and then multiplying by the power temperature coefficient of panel:

$$PR_{temperature\text{-}corrected} = (T_{Module} - 25 \text{ K}) \cdot k_t \tag{13}$$

$$PR_{STC} = PR - PR_{temperature\text{-}corrected} \tag{14}$$

with k_t the module temperature coefficient.

As to enable real-time monitoring, the above calculations need to be performed throughout the day. The final STC corrected *PR* usually concerns 15 minute periods, so module temperatures fluctuating during this time due to changing irradiance intensities will be averaged. The 15 minute averages have proved to be a good trade-off between data being too granular as to be useless for comparison, and data produced too late as to be of immediate use.

A drop in expected *PR* should trigger closer monitoring by the maintenance staff to ascertain its reason.

4.4.2 Recommendations to Inverter Manufacturers

When a drop in *PR* for an array or inverter is reported, the monitoring staff can then examine all the immediately available data in the monitoring system for the affected array or inverter. They can search for values in parameters that stray from the expected, and then look for the cause of such behavior.

The success of such a search is only as successful as the quality and quantity of elements or parameters available for searching. For consumers having purchased certain inverter brands, the possibility for effective monitoring is solely in the hands of the manufacturer. Successful efficiency monitoring and optimizing performance of the array, therefore, are entirely in the hands of that manufacturer, and the tools he has decided to employ. Experience has shown that such systems do not enjoy relatively high performance, particularly due to long time to repair caused by difficulties in ascertaining cause of fault.

The following issues with inverter monitoring currently plague those attempting to monitor effectively, and should be alleviated by the inverter manufacturers:

1. The availability of any and all inverter parameters to the monitoring entity. Some manufacturers make available a fine long list of useful parameters including everything from power to fan voltage, with a cornucopia of useful parameters in between. Other manufacturers offer only power, current and voltage.
2. Making available simple access to the inverters from third party applications. Some inverter manufacturers allow easy access to the parameters, some seem to practically forbid access by third party, allowing only a limited number of parameters to be manually downloaded from a proprietary site.
3. A single protocol for the naming of parameters across the range of products available from a single manufacturer.
4. A single protocol across the industry for the naming of parameters available for monitoring (authors note: such a protocol is in the making).
5. A standard for the accuracy of the monitored values, particularly the energy related values such as current and voltage. This standard should require metering accuracy of at least 1%.

4.4.3 Controlling the "Controllable" Factors in Performance Monitoring

The *PR* is useful to help mitigate some of the controllable factors listed above. The *PR* will drop over time once dust settles onto the modules and a soiling film evolves on the module cover. When cleaned, the *PR* rises. This difference is to be monitored and applied as a measure for when it is financially advantageous to clean the array though out the year. This is clearly a maintenance task.

Shading due to vegetation can be noticed in the monitoring system, particularly when strings are monitored. Occasional drops in string current with no drop in solar irradiance can point to shading due to growing vegetation (see examples in Section 2.2).

Another maintenance task that is not as obvious as cleaning of modules is related to ensuring good insulation properties of all arrays. Here, preventive maintenance is important to ensure quality of galvanic connections. Although as of today no correlation between monitored parameters and every possible faulty connection has been proven statistically, the initial work that has been undertaken in this area shows that monitoring array insulation would be beneficial in assuring the early detection of electrical system faults including fire hazards.

Surge arrestors are of great importance to ensuring longevity to the modules in the field or on the roof. It is strongly recommended that surge arrestors equipped with alarming contacts are used, and that these contacts are included in the monitoring system.

Inverter state-of-health parameters, such as interior temperature, fan voltage or time at work, if available, can aid in ascertaining blocked filters or other physical causes of stress to the inverter.

5   Conclusions

The present report provides detailed guidelines, methods and models for the analysis of the performance of PV systems. This includes effects related to special PV module technologies.

In particular, best practices in PV monitoring have been documented based on the scientific state-of-the-art and in line with common practices in the field. Guidelines and examples have been presented for visual analysis of PV monitoring data by means of collections of stamp-like plots. The mathematical approach of periodic linear regression has been elaborated. It allows for describing and analyzing the energy flow in a grid-connected photovoltaic system with a selected collection of variables describing the main energy conversion steps taking place in the system.

Effects related to special PV technologies, namely CIGS and amorphous silicon PV, have been studied in detail. Based on data from different experimental installations in the field, their specific behavior has been modeled and compared to classical crystalline silicon PV. In conclusion, for CIS technologies no major modifications to the existing models for crystalline silicon are required when modeling the output over a month or longer. For modules involving amorphous silicon, the existing models for crystalline silicon require major modifications in order to take into account the sensitivity to the spectral composition of the incoming light. Methods to take into account the spectral response in the absence of dedicated spectral measurements have been developed and tested. First results look promising, however, further scientific validation needs to be pursued. When ready for application, these models will allow for distinguishing the different causes for performance variations better, in particular between meteorological variations on the one hand and degradation or other changes in the solar cell material on the other hand.

Regarding system design decisions, the main factors of influence are mounting angle and row distance, related to irradiance gains and shading losses, inverter to module power ratio and cabling optimizations. Several examples on both shading losses and inverter to module power ratio were highlighted.

Regarding operational monitoring in real time, the basic approach of real-time data processing was described. Detailed recommendations are given, especially for inverter manufacturers, with inverter functions being central to achieving progress in the area of system optimization. Finally, measures that can help to improve the performance of PV systems have been described. The recommendations are based on lessons learned from PV system design as well as operational monitoring by means of real time data acquisition.

In conclusion, this report delivers a set of practical guidelines, methods and models that can be considered as best practices in the area of analytical monitoring of PV systems today. Systematically applied, they will contribute to further increase the performance of PV power plants also in the future.

References

[1]   "IEC 61724 Std. Photovoltaic System Performance Monitoring-Guidelines for Measurement, Data Exchange and Analysis." IEC, 1998.

[2]   G. Blaesser and D. Munro, "Guidelines for the Assessment of Photovoltaic Plants Document A Photovoltaic System Monitoring," Commission of the European Communities, Joint Research Centre, Ispra, Italy, EUR 16338 EN, Issue 4.2 (June 1993), 1995.

[3]   U. Jahn and W. Nasse, "Operational performance of grid-connected PV systems on buildings in Germany," *Prog. Photovolt. Res. Appl.*, vol. 12, no. 6, pp. 441–448, 2004.

[4]   S. Mau and U. Jahn, "Performance analysis of grid-connected PV systems," in *21st EUPVSEC*, Dresden, Germany, 2006, pp. 2676–2680.

[5]   U. Jahn, W. Nasse, T. Nordmann, L. Clavadetscher, and D. Mayer, "Achievements of task 2 of IEA PV power systems programme: final results on PV system performance," in *19th EUPVSEC*, Paris, France, 2004, pp. 2813–2816.

[6]   U. Jahn, D. Mayer, M. Heidenreich, R. Dahl, S. Castello, L. Clavadetscher, A. Frölich, B. Grimmig, W. Nasse, and K. Sakuta, "International Energy Agency PVPS Task 2: Analysis of the operational performance of the IEA Database PV systems," in *16th EUPVSEC*, Glasgow, United Kingdom, 2000, pp. 2673–2677.

[7]   G. Blaesser and D. Munro, "Guidelines for the Assessment of Photovoltaic Plants Document B Analysis and Presentation of Monitoring Data," Commission of the European Communities, Joint Research Centre, Ispra, Italy, EUR 16339 EN, Issue 4.1 (June 1993), 1995.

[8]   M. Sengupta, P. Gotseff, and T. Stoffel, "Evaluation of Photodiode and Thermopile Pyranometers for Photovoltaic Applications," in *27th EUPVSEC*, Frankfurt, Germany, 2012, pp. 3705–3708.

[9]   S. Reinhardt, C. Eggers, S. Grünsteidl, and C. Vodermayer, "Influence of Technology Differences in Performance Ratio Calculations," in *27th EUPVSEC*, Frankfurt, Germany, 2012, pp. 4025 – 4026.

[10]   N. Pearsall and B. Atanasiu, "The European PV system monitoring guidelines-Modernisation under the PERFORMANCE project," in *Photovoltaic Specialists Conference (PVSC), 2009 34th IEEE*, Philadelphia, PA, 2009, pp. 000256–000261.

[11]   N. Pearsall, B. Atanasiu, and T. Huld, "The European PV System Monitoring Guidelines - Summary and Implementation," in *25th EUPVSEC / 5th World Conference on Photovoltaic Energy Conversion*, Valencia, Spain, 2010, pp. 5055–5061.

[12]   N.M. Pearsall and B. Atanasiu, "Assessment of PV System Monitoring Requirements by Consideration of Failure Mode Probability," in *24th EUPVSEC*, Hamburg, Germany, 2009, pp. 3896 – 3903.

[13]   T. Oozeki, T. Izawa, K. Otani, and K. Kurokawa, "An evaluation method of PV systems," *Sol. Energy Mater. Sol. Cells*, vol. 75, no. 3, pp. 687–695, 2003.

[14]   S. Stettler, P. Toggweiler, E. Wiemken, W. Heydenreich, A. C. de Keizer, W. van Sark, S. Feige, M. Schneider, G. Heilscher, and E. Lorenz, "Failure detection routine for grid-connected PV systems as part of the PVSAT-2 project," in *20th EUPVSEC*, Barcelona, Spain, 2005, pp. 2490–2493.

[15]   A. Drews, A. C. De Keizer, H. G. Beyer, E. Lorenz, J. Betcke, W. Van Sark, W. Heydenreich, E. Wiemken, S. Stettler, and P. Toggweiler, "Monitoring and remote failure detection of grid-connected PV systems based on satellite observations," *Sol. Energy*, vol. 81, no. 4, pp. 548–564, 2007.

[16]   A. C. de Keizer, W. van Sark, S. Stettler, P. Toggweiler, E. Lorenz, A. Drews, D. Heinemann, G. Heilscher, M. Schneider, and E. Wiemken, "PVSAT-2: Results of field test of the satellite-based PV system performance check," in *Proc. 21st European Photovoltaic Solar Energy Conference, Dresden*, 2006, pp. 4–8.

[17]   Carl Von Ossietzky Universitat Oldenburg, "PVSAT-2," *PVSAT-2: Weather satellites help improving PV system performance*, 10-Jul-2009. [Online]. Available: http://www.energy-meteorology.de/17967.html.

[18]   Y. Ueda, K. Kurokawa, K. Kitamura, M. Yokota, K. Akanuma, and H. Sugihara, "Performance analysis of various system configurations on grid-connected residential PV systems," *Sol. Energy Mater. Sol. Cells*, vol. 93, no. 6, pp. 945–949, 2009.

[19] S. J. Ransome, J. H. Wohlgemuth, S. Poropat, and E. Aguilar, "Advanced analysis of PV system performance using normalised measurement data," in *Conference Record of the Thirty-first IEEE Photovoltaic Specialists Conference*, 2005, pp. 1698–1701.

[20] S. Sellner, J. Sutterlüti, S. Ransome, L. Schreier, and N. Allet, "Understanding PV module performance: further validation of the novel loss factors model and its extension to AC arrays," in *27th EU PVSEC*, Frankfurt, Germany, 2012, pp. 3199–3204.

[21] "Integrated Project 'Performance', FP6, D1.3.2 Guideline for the use of reference devices: (I) Basic considerations and recommendations," Fraunhofer-Institut für Solare Energiesysteme, ISE, Jul. 2007.

[22] A. Guerin de Montgareuil, "A New Accurate Method for Outdoor Calibration of Field Pyranometers," in *19th EUPVSEC*, Paris, France, 2004.

[23] Kipp & Zonen, "Calibration certificate pyranometer CMP11 (007680128598) and (007680128603)." Kipp & Zonen, 30-Oct-2012.

[24] Kipp & Zonen, "CMP Pyranometers - Brochure (CMP 3, CMP 6, CMP 11, CMP 21 and CMP 22)." 2013.

[25] T. Betts, Bliss, M, Gottschlg, R, and Infield, D.G, "Consideration of Error Sources for Outdoor Performance Testing of Photovoltaic Modules," in *20th EUPVSEC*, Barcelona, Spain, 2005.

[26] A. Spena, C. Cornaro, G. Intreccialagli, and D. Chianese, "Data validation and uncertainty evaluation of the ester outdoor facility for testing of photovoltaic modules," in *24th EUPVSEC*, Hamburg, Germany, 2009.

[27] NASA, "NASA Satellite data," *Surface meteorology and Solar Energy*. [Online]. Available: https://eosweb.larc.nasa.gov/sse/.

[28] S. Ransome, "How well do PV modelling algorithms really predict performance?," in *22nd EUPVSEC*, Milano, Italy, 2007.

[29] "Fraunhofer IWES Calibration certificate for ISET-Sensor." .

[30] T. Glotzbach, B. Schulz, M. Zehner, P. Fritze, M. Schlatterer, C. Vodermayer, G. Wotruba, and M. Mayer, *„Round-Robin-Test of Irradiance Sensors "*. 24th PVSEC, Valencia (Spain), 2008.

[31] M. Zehner, P. Fritze, M. Schlatterer, T. Glotzbach, B. Schulz, C. Vodermayer, M. Mayer, and G. Wotruba, "One year round robin testing of irradiation sensors measurement results and analyses," in *24th EUPVSEC*, Hamburg, Germany, 2009.

[32] B. Müller, C. Reise, W. Heydenreich, and K. Kiefer, "Are Yield Certificates Reliable?: A Comparison to Monitored Real World Results," in *22nd EUPVSEC*, Milano, Italy, 2007.

[33] N. H. Reich, B. Mueller, A. Armbruster, W. G. J. H. M. van Sark, K. Kiefer, and C. Reise, "Performance ratio revisited: is PR > 90% realistic?," *Prog. Photovolt. Res. Appl.*, vol. 20, no. 6, pp. 717–726, 2012.

[34] J. Meydbray, E. Riley, L. Dunn, K. Emery, and S. Kurtz, "Pyranometers and Reference Cells: Part 2: What Makes the Most Sense for PV Power Plants?," Oct. 2012.

[35] "ISO 9060:1990 Solar energy -- Specification and classification of instruments for measuring hemispherical solar and direct solar radiation." .

[36] D. Dirnberger and U. Kraling, "Uncertainty in PV Module Measurement - Part I: Calibration of Crystalline and Thin-Film Modules," *IEEE J. Photovolt.*, vol. 3, no. 3, pp. 1016–1026, 2013.

[37] S. Winter, "Personal communication with S. Winter of PTB, Germany."

[38] D. Dirnberger, J. Barkte, A. Steinhüser, K. Kiefer, and F. Neuberg, "Uncertainty of Field I-V Curve Measurements in Large Scale PV Systems," in *25th EUPVSEC / 5th World Conference on Photovoltaic Energy Conversion*, Valencia, Spain, 2010, pp. 4587–4594.

[39] A. Virtuani, H. Muellejans, F. Ponti, and E. Dunlop, "Comparison of Indoor and Outdoor Performance Measurements of Recent Commercially Available Solar Modules," in *23rd European Photovoltaic Solar Energy Conference*, Valencia, Spain, 2008.

[40] W. Herrmann, S. Zamini, F. Fabero, T. Betts, N. van der Borg, K. Kiefer, G. Friesen, and W. Zaaiman, "Results of the European PERFORMANCE project on the development of measurement techniques for thin-film PV modules," in *23rd EUPVSEC*, Valencia, Spain, 2008.

[41] "ISO/TR 9901:1990 Solar energy -- Field pyranometers -- Recommended practice for use." .

[42] P. Ineichen, "Five satellite products deriving beam and global irradiance validation on data from 23 ground stations," University of Geneva, Geneva, Switzerland, Scientific report, 2011.

[43] S. Ransome and P. Funtan, "Why hourly averaged measurement data is insufficient to model PV system performance accurately," in *20th European Photovoltaic Solar Energy Conference and Exhibition*, Barcelona, Spain, 2005, pp. 2752–2755.

[44] A. Woyte, M. Richter, D. Moser, S. Mau, N. H. Reich, and U. Jahn, "Monitoring of Photovoltaic Systems: Good Practices and Systematic Analysis," in *Proc. 28th European Photovoltaic Solar Energy Conference*, Paris, France, 2013, pp. 3686–3694.

[45] "PV Performance Modeling Collaborative," *PV Performance Modeling Collaborative*. [Online]. Available: http://pvpmc.org/. [Accessed: 25-Jul-2013].

[46] A. Luque and S. Hegedus, *Photovoltaic Science and Engineering*. Wiley, 2003.

[47] J. A. Duffie and W. A. Beckman, *Solar engineering of thermal processes*. Wiley, 1991.

[48] D. L. King, W. E. Boyson, and J. A. Kratochvil, "Photovoltaic Array Performance Model," Sandia National Laboratories, Albuquerque, New Mexico, Unlimited Release SAND2004-3535, 2004.

[49] G. Belluardo, M. Pichler, D. Moser, and M. Nikolaeva, "One-year comparison of different thin film technologies at Bolzano Airport Test Installation," in *Fuelling the Future: Advances in Science and Technologies for Energy Generation, Transmission and Storage*, Universal-Publishers, 2012, pp. 229–234.

[50] D. Moser, M. Pichler, and M. Nikolaeva-Dimitrova, "Filtering Procedures for Reliable Outdoor Temperature Coefficients in Different Photovoltaic Technologies," *J. Sol. Energy Eng.*, vol. 136, no. 2, Aug. 2013.

[51] H. G. Beyer, G. H. Yordanov, O.-M. Midtgård, T. O. Sætre, and A.-G. Imenes, "Contribution to the konwledge base on PV performance: evaluation of the operation of PV Systems using different technologies in Southern-Norway," presented at the 37th PVSC, Seattle, USA, 2011.

[52] H. G. Beyer, A. McKinley, and G. H. Yordanov, "Gleichmäßigkeit des Betriebsverhaltens von Dünnschicht-Modulen," presented at the 27th Symp. Photovoltaische Solarenergie, Bad Staffelstein, Germany, 2012.

[53] H. G. Beyer and G.H.Yordanov, "Stability of the performance of thin film modules during one year of operation," in *Photovoltaic Specialists Conference (PVSC), 2012 38th IEEE*, Austin, USA, 2012, pp. 002391–002394.

[54] H. G. Beyer, "Nachverfolgung des Betriebsverhaltend von Dünnschicht Modulen im Rahmen der IEA PVPS Task13," presented at the 29th Symp. Photovoltaische Solarenergie, Bad Staffelstein, Germany, 2013.

[55] H. G. Beyer, T. O. Saetre, and G. H. Yordanov, "Using broad-band irradiance data to model the short circuit response of aSi modules," presented at the 37th PVSC, Tampa, USA, 2013.

[56] D. L. King, "More 'efficient' methods for specifying and monitoring PV system performance," presented at the 37th IEEE Photovoltaic Specialists Conference (PVSC), Seattle, WA, 2011, pp. 219–224.

[57] B. Decker and U. Jahn, "Performance of 170 grid connected PV plants in northern Germany—analysis of yields and optimization potentials," *Sol. Energy*, vol. 59, no. 4, pp. 127–133, 1997.

[58] B. Marion, J. Adelstein, K. Boyle, H. Hayden, B. Hammond, T. Fletcher, D. Narang, A. Kimber, L. Mitchell, and G. Rich, "Performance parameters for grid-connected PV systems," in *Conference Record of the Thirty-first IEEE Photovoltaic Specialists Conference*, 2005, pp. 1601–1606.

[59] L. Maturi, "Building skin as energy supply: Prototype development of a wooden prefabricated BiPV wall," University of Trento, 2013.

[60] B. P. Koirala, B. Sahan, and N. Henze, "Study on MPP mismatch losses in photovoltaic applications," in *24th EUPVSEC*, Hamburg, Germany, 2009, pp. 3727–3733.

[61] J. Leloux, L. Narvarte, and D. Trebosc, "Review of the performance of residential PV systems in France," *Renew. Sustain. Energy Rev.*, vol. 16, no. 2, pp. 1369–1376, 2012.

[62] J. Leloux, L. Narvarte, and D. Trebosc, "Review of the performance of residential PV systems in Belgium," *Renew. Sustain. Energy Rev.*, vol. 16, no. 1, pp. 178–184, Jan. 2012.

[63] H. S. Huang, J. C. Jao, K. L. Yen, and C. T. Tsai, "Performance and Availability Analyses of PV Generation Systems in Taiwan," *World Acad. Sci. Eng. Technol.*, vol. 54, 2011.

[64] J. Leloux, L. Narvarte Fernandez, and D. Trebosc, "Performance Analysis of 10,000 Residential PV Systems in France and Belgium," in *26th EUPVSEC*, Hamburg, Germany, 2011, pp. 3939–3946.

[65] D. C. Jordan and S. R. Kurtz, "Photovoltaic degradation rates—an analytical review," *Prog. Photovolt. Res. Appl.*, vol. 21, no. 1, pp. 12–29, Jun. 2012.

[66] E. Alsema, D. Fraile, R. Frischknecht, V. Fthenakis, M. Held, H. C. Kim, W. Pölz, M. Raugei, and M. de Wild Scholten, "Methodology guidelines on life cycle assessment of photovoltaic electricity," International Energy Agency Photovoltaic Power Systems Programme, IEA PVPS T12-01:2009, Oct. 2009.

[67] J. H. Wohlgemuth and B. P. Solar, "Long term photovoltaic module reliability," in *National Center for Photovoltaics and Solar Program Review Meeting Proceedings 2003*, 2003.

[68] B. Müller, U. Kräling, W. Heydenreich, Ch. Reise, and K. Kiefer, "Simulation of irradiation and temperature dependent efficiency of thin film and crystalline silicon modules based on different parameterization," in *25th EUPVSEC / 5th World Conference on Photovoltaic Energy Conversion*, Valencia, Spain, 2010, pp. 4240–4243.

[69] S. Dittmann, G. Friesen, S. Williams, T. R. Betts, R. Gottschalg, H. G. Beyer, and A. G. de Montgareuil, "Results of the 3rd Modelling Round Robin Within the European Project 'PERFORMANCE' - Comparison of Module Energy Rating Methods," in *25th EUPVSEC*, Valencia, Spain, 2010, pp. 4333–4338.

[70] R. Perez, P. Ineichen, R. Seals, J. Michalsky, and R. Stewart, "Modeling Daylight Availability and Irradiance Components from Direct and Global Irradiance," *Sol. Energy*, vol. 44, no. 5, pp. 271–289, 1990.

[71] B. Müller, Th. Reis, A. Driesse, and Ch. Reise, "Maximizing the Yield of Large PV Power Plants: What Can We Learn From Monitoring and Simulation?," in *27th EU PVSEC*, Frankfurt, Germany, 2012, pp. 3775–3781.

[72] Stephan.Elies, Thomas Reis, Björn Müller, Ulli Kräling, and Klaus Kiefer, "Influence of row-shading on the performance of PV systems – simulation and measurement," in *25th EUPVSEC*, Valencia, Spain, 2010, pp. 4640–4646.

[73] K. Kiefer and et al., "A degradation analysis of PV power plants," in *25th EUPVSEC*, Valencia, Spain, 2010, pp. 5032–5037.

[74] I. Reda, "Method to calculate uncertainties in measuring shortwave solar irradiance using thermopile and semiconductor solar radiometers," *Contract*, vol. 303, pp. 275–3000, 2011.

[75] C. A. Gueymard and D. R. Myers, "Evaluation of conventional and high-performance routine solar radiation measurements for improved solar resource, climatological trends, and radiative modeling," *Sol. Energy*, vol. 83, no. 2, pp. 171–185, 2009.

[76] M. A. Muñoz-García, O. Marín González, A. Garcia, M. Carmen, and F. Chenlo, "Thim Films Modules Characterization Under Standard Test Conditions," in *25th EUPVSEC / 5th World Conference on Photovoltaic Energy Conversion*, Valencia, Spain, 2010, pp. 4378–4382.

[77] J. A. del Cueto, C. A. Deline, D. S. Albin, S. R. Rummel, and A. Anderberg, "Striving for a standard protocol for preconditioning or stabilization of polycrystalline thin film photovoltaic modules," in *SPIE 7412, Reliability of Photovoltaic Cells, Modules, Components, and Systems II*, San Diego, California, United States, 2009, vol. 7412.

[78] Arndt R. and Puto R, "Basic Understanding of IEC Standard Testing for Photovoltaic Panels." Compliance Magazine, 2010.

[79] T. Sample, "Preconditioning of Thin-Film PV Modules Through Controlled Light-Soaking," in *NREL Photovoltaic Module Reliability Workshop*, 2012.

[80] C. Deline, A. Stokes, T. J. Silverman, S. Rummel, D. Jordan, and S. Kurtz, "Electrical bias as an alternate method for reproducible measurement of copper indium gallium diselenide (CIGS) photovoltaic modules," in *SPIE Optics + Photonics*, San Diego, California, United States, 2012, p. 84720G–84720G.

[81] C. Deline, D. S. Albin, and S. Rummel, "Metastable electrical characteristics of polycrystalline thin-film photovoltaic modules upon exposure and stabilization," *J. Photonics Energy*, vol. 2, no. 1, pp. 022001–1, 2012.

[82] IEA PVPS Task 2, "Cost and Performance Trends in Grid-Connected Photovoltaic Systems and Case Studies," International Energy Agency Photovoltaic Power Systems Programme, IEA-PVPS T2-06:2007, 2007.

[83] H. Haeberlin and C. Beutler, "Normalized Representation of Energy and Power for Analysis of Performance and on-line Error Detection in PV-Systems," in *Proc. 13th EU PV Conf., Nice*, 1995.

[84] IEC, "IEC 60364-7-712 Std. Electrical installation of buildings - Part 7-712: Requirements for special installations or locations - Solar photovoltaics (PV) power supply systems," *Int. Electro-Tech. Comm.*, 2002.

Annex A: List of Example Installations

No.	Location	Monitored / data / figures by	Installed power [kWp]	Tilt	Azimuth (S=180°)	PV technology	Mounting	Text Reference
BE1	Belgium	3E	900	10°	180°	Crystalline silicon	Open field – fixed rack	Figure 8
CA1	Canada	PV Performance Labs	19.8	70°	186°	Crystalline silicon	Facade/awning	Figure 18
ES1	Southern Spain	GL Garrad Hassan	1.15	30°	180°	Crystalline silicon	Open field – fixed rack	Figure 19
FR1	France	INES	35.2	20°	270°	Crystalline silicon	Roof integrated	Figure 21
IT1	Italy	EURAC	4.14	30°	188.5°	Crystalline silicon	Open field – fixed rack	Figure 15, Figure 17
IT2	Italy	EURAC	1.10	30°	188.5°	CIGS	Open field – fixed rack	Figure 20
MY1	Malaysia	University Teknologi MARA	0.9	15°	180°	Amorphous silicon	Flat roof – Free standing	Figure 14
MY2	Malaysia	University Teknologi MARA	6.11	15°	180°	Crystalline silicon	Retrofitted on metal-deck roof	Figure 14
NO1	Southern Norway	Teknova	5.4	20°	200°	Crystalline silicon	Flat roof – free standing	Figure 10
NO2	Southern Norway	Teknova	2.4	20°	200°	Tandem Crystalline/ Amorphous Silicon	Flat roof – free standing	Figure 16, Figure 22
SE1	Västerås, Sweden	ABB	3.0	40°	194°	Crystalline silicon	Open field – fixed rack	Figure 9, Figure 11
SE2	Stockholm, Sweden	KTH Royal Institute of Technology	10.08	42°	180°	Crystalline silicon	Roof (good ventilation)	Figure 12, Figure 13, Figure 22 (a)

Annex B: Definitions

Following, Table 12 presents an overview of the recorded and derived parameters for performance evaluation.

Table 12: Recorded parameters for performance evaluation of grid-connected PV systems (adapted and extended from [1] and [82])

Parameter	Symbol	Unit
Plant data		
Nominal power / peak power	P_0	W
STC reference irradiance (1000 W/m^2)	G_{STC}	W/m^2
STC reference temperature (25 °C)	T_{STC}	°C
PV array voltage at STC	V_{STC}	V
Temperature coefficient of power	γ	K^{-1}
Temperature coefficient of voltage	β	K^{-1}
Recorded parameters		
In-plane irradiance	G_I	W/m^2
Ambient temperature	T_{amb}	°C
Module temperature	T_{mod}	°C
Wind speed	S_w	m/s
(normalized) PV array output voltage	v_{DC}, V_{DC}	p.u., V
PV array output power	P_{DC}	kW
(normalized) utility grid voltage	v_{AC}, V_{AC}	p.u., V
Power to utility grid	P_{AC}	kW
Non-availability of the PV system	t_{NAV}	h
Total duration of the monitoring activity	τ	h
Derived parameters		
In-plane irradiation	H_I	Wh/m^2
PV array energy output	E_{DC}	kWh
Energy to utility grid	E_{AC}	kWh
(Instantaneous)* reference yield	y_r, Y_r	- , h
(Instantaneous)* array yield	y_A, Y_A	- , h
(Instantaneous)* system yield	y_f, Y_f	- , h
(Instantaneous)* array capture losses	l_C, L_C	- , h
(Instantaneous)* system losses	l_S, L_S	- , h
Equivalent thermal resistance	k_{th}	K/(W/m^2)
Equivalent thermal resistance without wind	$k_{th,0}$	K/(W/m^2)
Coefficient for thermal convection	C_{th}	-
Virtual grid impedance	z	p.u.
(Instantaneous)* performance ratio	pr, PR	- or %
Average performance ratio (over different samples)	$\overline{pr}$	- or %
(Instantaneous)* array performance ratio	pr, PR	- or %
Average array performance ratio (over different samples)	$\overline{pr}$	- or %
Outage fraction	O	- or %

* For the classical yield and loss quantities we use small letters when referring to instantaneous values or averages over a short recording period.

The *instantaneous* values as presented in Table 12 are calculated by normalizing the corresponding energy values (yields and losses) to the recording period over which the recorded samples have been averaged. Physically, they are averages over the recording period, which approximate the instantaneous values. The shorter the recording period, the better is the approximation. The period should be no longer than one hour. In practice, these data are usually treated as instantaneous values and they reflect irradiance and power rather than irradiation or energy. As stated in [83], these quantities allow a much more detailed analysis of system performance and are very useful for on-line error detection by using data collected with a high resolution, e.g. every second.

The derived parameters presented in Table 12 are briefly described below in line with [3], [1], [84].

Reference yield (Y_r)

$$Y_r = \frac{H_I}{G_{STC}} \qquad (15)$$

Instantaneous reference yield (y_r)

$$y_r = \frac{G_I}{G_{STC}} \qquad (16)$$

Array yield (Y_A)

$$Y_A = \frac{E_{DC}}{P_o} \qquad (17)$$

Instantaneous array yield (y_A)

$$y_A = \frac{P_{DC}}{P_o} \qquad (18)$$

P_{DC} is the is the measured DC power of the system [kW]

Capture losses (L_C)

$$L_C = Y_r - Y_A \qquad (19)$$

Instantaneous array capture losses (l_C)

$$l_C = y_r - y_A \qquad (20)$$

System yield (Y_f)

$$Y_f = \frac{E_{AC}}{P_o} \qquad (21)$$

Instantaneous system yield (y_f)

$$y_f = \frac{P_{AC}}{P_o} \qquad (22)$$

System losses (L_S)

$$L_S = Y_A - Y_f \qquad (23)$$

Instantaneous system losses (l_S)

$$l_S = y_A - y_f \qquad (24)$$

Performance ratio (PR)

$$PR = \frac{Y_f}{Y_r} \qquad (25)$$

Instantaneous performance ratio (pr)

$$pr = \frac{y_f}{y_r} \qquad (26)$$

Array performance ratio (PR)

$$PR_A = \frac{Y_A}{Y_r} \qquad (27)$$

Instantaneous array performance ratio (pr)

$$pr_A = \frac{y_A}{y_r} \qquad (28)$$

Outage fraction

$$O = \frac{t_{outage}}{\tau} \qquad (29)$$

For further information about the IEA – Photovoltaic Power Systems Programme and Task 13 publications, please visit www.iea-pvps.org.